Available online at www.sciencedirect.com
ScienceDirect
Comput. Methods Appl. Mech. Engrg. 333 (2018) 94–113
Computer methods in applied mechanics and engineering
www.elsevier.com/locate/cma

A random field model for anisotropic strain energy functions and its application for uncertainty quantification in vascular mechanics

B. Staber[a,b], J. Guilleminot[a,*]

[a] *Department of Civil and Environmental Engineering, Duke University, Durham, NC 27708, USA*
[b] *Université Paris-Est, Laboratoire Modélisation et Simulation Multi Echelle, MSME UMR 8208 CNRS, Marne-la-Vallée, France*

Received 7 June 2017; received in revised form 2 October 2017; accepted 2 January 2018
Available online 31 January 2018

Abstract

This paper deals with the construction of random field models for spatially-dependent anisotropic strain energy functions indexed by complex geometries. The approach relies on information theory and the principle of maximum entropy, which are invoked in order to construct the family of first-order marginal probability distributions in accordance with fundamental constraints such as polyconvexity, coerciveness and consistency at small strains. We then address the definition of a sampling methodology able to perform on domains that are non-homotopic to a sphere, with the aim to generate the non-Gaussian random fields on non-simplified geometries—such as patient-specific geometries in computational biomechanics. The algorithm is based on the construction of a diffusion field that involves local geometrical features of the manifolds defining domain boundaries. We finally present numerical applications on vascular tissues, including the case of an arterial wall defined by real patient-specific data.

Keywords: Stochastic modeling; Hyperelasticity; Nonlinear elasticity; Soft biological tissues; Entropy; Uncertainty quantification

1. Introduction

The mathematical representation of uncertainties is a key ingredient in predictive science and engineering [1]. In continuum mechanics, uncertainties in constitutive laws can arise from subscale (morphological) randomness, especially when the so-called separation of scales does not hold [2], or from fluctuations in the properties of the constitutive phases. This variability can notably be inherited from processing in the case of engineered composites, or from various factors including age, gender or physiological state when biological tissues are concerned. Experimental evidences of stochasticity in the response of biological tissues can be found in e.g. [3–14]. In this context, the question as to how properly model, identify and simulate such randomness is a central challenge in both computational mechanics and mechanics of materials.

* Corresponding author.
E-mail address: johann.guilleminot@duke.edu (J. Guilleminot).

https://doi.org/10.1016/j.cma.2018.01.001

Within the framework of uncertainty quantification [15,16], popularized by the seminal work from Ghanem and Spanos [17], this stochastic modeling task has been mostly addressed by resorting to polynomial chaos expansions (PCE) [18,19] of random variables [20,21] and random fields [22]. In particular, detailed derivations focusing on the PCE-based representation of tensor-valued coefficients for stochastic elliptic operators (hence encompassing the case of linear elasticity) can be found in the recent work [23]. Statistical approaches based on Bayesian inference have also received considerable attention, with the promise to accommodate data paucity through data-driven methodologies [1] (see also [24] for an application to PCE). Algebraic decompositions of random fields for stochastic three-dimensional elasticity were further constructed in [25–30] and validated on various multiscale or multimodel problems in e.g. [31–33]. Spectral expansions for elasticity random fields were finally obtained in [34] for all material symmetry classes.

In contrast, the construction of stochastic models in nonlinear elasticity has received much less consideration to date, and most of the efforts were basically focused on the propagation of PCE through nonlinear computational models (see e.g. [35,36] for applications in elastoplasticity). A noticeable contribution relying on a Bayesian formulation and accounting for both spatial variability and non-simplified domains can be found in [37]. Here, a parameter defining the isotropic strain energy function of interest is modeled as a non-Gaussian (translation) random field for which (i) the first-order marginal probability function is selected a priori; (ii) the covariance (exponential) kernel defining the underlying centered Gaussian field is chosen with no reliance on the geometry (see also [38]). The construction of information-theoretic stochastic models for random isotropic strain energy functions was recently tackled in [39–41] (see the references therein for surveys), for both compressible and incompressible materials. These models, which can appropriately be used in order to define first-order marginal probability laws for random fields, were further identified and validated with experiments on various soft biological tissues (including brain and liver tissues, as well as spinal cord white matter) in [41].

The aim of this paper is to address the construction of a prior stochastic model for spatially-dependent anisotropic strain energy functions. Such a prior model essentially allows *admissible* samples of the strain energy functions to be drawn, in accordance with fundamental theoretical results in finite elasticity, and can subsequently be used to solve underdetermined statistical inverse problems or combined with Bayesian approaches [42]. Envisioned applications include large-scale computational analysis in biomechanics, particularly for soft biological tissues such as vascular vessels, and the modeling of composite materials at large strains. This construction raises two main challenging issues. First of all, the consideration of anisotropic strain energy functions leads to higher-dimensional parametrizations and more complex constraints between the variables. In addition, it requires the construction of stochastic models for non-Gaussian vector-valued random fields. Second, the simulation of these models necessitates describing the correlation structure and sampling the random fields on non-simplified geometries where boundaries typically take the form of smooth manifolds.

The rest of this paper is organized as follows. The fundamentals of continuum mechanics and hyperelasticity are first briefly exposed in Section 2. In particular, the definition of a prototypical strain energy function is presented, and theoretical requirements raised by the analysis of the nonlinear boundary value problems are highlighted. The stochastic framework is next introduced in Section 3. Here, a new random field model is derived within the framework of information theory. This probabilistic modeling effort is subsequently complemented, in Section 4, with the definition of a sampling methodology. The computational approach relies on solving a stochastic partial differential equation, the coefficients of which are specifically defined in accordance with the geometry under consideration. This allows, in particular, the case of non-simplified domains to be handled in an efficient and robust manner. Various applications, including the case of an arterial wall defined by a patient-specific geometry and undergoing inner pressure, are finally presented in Section 5 to assess and illustrate the modeling capability of the proposed stochastic framework and algorithms.

2. Deterministic modeling of anisotropic hyperelastic materials

2.1. Kinematics

In this section, we recall the continuum mechanics framework that is relevant to the modeling of anisotropic materials at finite strains. The interested reader is referred to classical textbooks (e.g. [43–45]) for a more extensive exposure.

Let $\mathscr{B}$ denote a fixed stress-free reference configuration occupied by a body $\mathscr{P}$ in $\mathbb{R}^3$, with boundary $\partial\mathscr{B}$. The body undergoes a deformation $\boldsymbol{\varphi} : \mathscr{B} \to \mathscr{D}$, where $\mathscr{D}$ is the deformed configuration and $\boldsymbol{\varphi}$ belongs to some suitable space $\mathscr{C}$ [43]. Any material point in the reference configuration is identified with its position vector $\mathbf{x}$. Following standard notation, the deformation gradient is defined as $\mathsf{F}(\mathbf{x}) := \nabla_{\mathbf{x}}\boldsymbol{\varphi}(\mathbf{x})$, with $\det(\mathsf{F}(\mathbf{x})) > 0$, and the right Cauchy tensor is denoted by $\mathsf{C}(\mathbf{x}) := \mathsf{F}(\mathbf{x})^{\mathrm{T}}\mathsf{F}(\mathbf{x})$. The associated Green–Lagrange deformation tensor E is defined as $\mathsf{E}(\mathbf{x}) := (\mathsf{C}(\mathbf{x}) - \mathsf{I})/2$. The body of interest is typically assumed to exhibit a hyperelastic response, characterized by the stored energy function $w : \mathscr{B} \times \mathbb{M}_3^+ \to \mathbb{R}$ (with $\mathbb{M}_3^+$ the set of (3×3) real matrices with strictly positive determinant). The function w is assumed to be frame-invariant, so that there exists a stored energy function $\widetilde{w} : \mathscr{B} \times \mathbb{S}_3^+ \to \mathbb{R}$ such that $\widetilde{w}(\mathbf{x}, \mathsf{C}) = w(\mathbf{x}, \mathsf{F})$ for all right Cauchy tensor $\mathsf{C} = \mathsf{F}^{\mathrm{T}}\mathsf{F}$ (here, $\mathbb{S}_3^+$ is the set of symmetric positive-definite real matrices of order 3).

Once the functional form of the strain energy function has been selected, the local constitutive equations can be formulated in terms of the second Piola–Kirchhoff stress tensor $\mathsf{S} : \mathscr{B} \times \mathbb{S}_3^+ \to \mathbb{S}_3^+$, defined as

$$\mathsf{S}(\mathbf{x}, \mathsf{C}) := 2D_C\widetilde{w}(\mathbf{x}, \mathsf{C}) = 2\frac{\partial \widetilde{w}(\mathbf{x}, \mathsf{C})}{\partial \mathsf{C}_{ij}}\mathbf{e}^{(i)} \otimes \mathbf{e}^{(j)} , \tag{1}$$

where Einstein summation convention is used (this convention is adopted from now on). The fourth-order tangent modulus tensor $[\![L]\!]$ is given by

$$[\![L(\mathbf{x}, \mathsf{C})]\!] := 4D_C^2\widetilde{w}(\mathbf{x}, \mathsf{C}) = 4\frac{\partial^2 \widetilde{w}(\mathbf{x}, \mathsf{C})}{\partial \mathsf{C}_{ij}\partial \mathsf{C}_{k\ell}}\,\mathbf{e}^{(i)} \otimes \mathbf{e}^{(j)} \otimes \mathbf{e}^{(k)} \otimes \mathbf{e}^{(\ell)} , \tag{2}$$

with $\{\mathbf{e}^{(i)}\}_{i=1}^3$ the canonical basis of $\mathbb{R}^3$, while the Cauchy stress tensor $\sigma : \mathscr{B} \times \mathbb{M}_3^+ \to \mathbb{S}_3$ is obtained as

$$\sigma(\mathbf{x}, \mathsf{F}) = \frac{1}{\det(\mathsf{F})}D_{\mathsf{F}}w(\mathbf{x}, \mathsf{F})\mathsf{F}^{\mathrm{T}} = \frac{1}{\det(\mathsf{F})}\mathsf{F}\mathsf{S}(\mathbf{x}, \mathsf{F}^{\mathrm{T}}\mathsf{F})\mathsf{F}^{\mathrm{T}} . \tag{3}$$

In this work, we focus our attention on anisotropic materials, in which case the stored energy function $\widetilde{w}$ satisfies the additional invariance property

$$\widetilde{w}(\mathbf{x}, \mathsf{C}) = \widetilde{w}(\mathbf{x}, \mathsf{Q}^{\mathrm{T}}\mathsf{C}\mathsf{Q}) , \quad \forall\, \mathsf{Q} \in \mathscr{G} , \tag{4}$$

where $\mathscr{G}$ denotes the symmetry group under consideration. The construction of such anisotropic models has recently attracted much attention, and various applications focusing on soft biological tissues can be found in e.g. [46–50] (see [51] for a recent survey). As for the case of isotropic models, admissible anisotropic models are required to satisfy mathematical constraints related to the existence of solutions for the associated nonlinear boundary value problem [43], as well as constraints raised by physical and phenomenological consistency. The first set of constraints involve, in most of the settings derived thus far, polyconvexity arguments [52] and suitable growth conditions that together ensure that either the total potential energy or the associated variational functional is sequentially weakly lower semicontinuous and coercive [53]. The second set of constraints usually involves invariance properties with respect to the action of a group of isometries, hence characterizing the underlying anisotropy, the consideration of prestressed or stress-free configurations at rest and asymptotic behaviors at vanishing and infinite strain states. In particular, the consideration of phenomenological aspects and experimental fitting concerns has led to the construction of a large variety of models (see the aforementioned references and the references therein). It should then be noticed that this work does not aim at providing a review on such deterministic models, nor at deriving stochastic extensions for all of them. Adopting a more constructive approach, this paper is alternatively concerned with the probabilistic extension of a given anisotropic functional form that is, on the one hand, representative of most anisotropic formulations, and on the other hand raises all the technical issues which could be faced while considering any other strain energy function. The definition of this prototypical strain energy function is addressed in the next section.

2.2. Selection of a prototypical anisotropic constitutive model

Hereinafter, we consider the case of anisotropic hyperelastic materials exhibiting two non-orthogonal preferred directions, defined by the vector fields $\mathbf{x} \mapsto \mathbf{a}^{(\ell)}(\mathbf{x})$, $\ell = 1, 2$, and schematically identified with the directions of two families of aligned fiber. This case is especially relevant to the modeling of arterial walls in computational

biomechanics (see Section 5.3) and allows the case of transversely isotropic composite plies to be recovered (by selecting $\mathbf{a}^{(1)}(\mathbf{x}) = \mathbf{a}^{(2)}(\mathbf{x}) = \mathbf{a}$ for all $\mathbf{x}$ in $\mathscr{B}$). The construction of a suitable form for the strain energy function is based on the earlier works in [46,54] (see also [55] for a discussion about the volumetric–isochoric multiplicative decomposition), and relies on the definition of fields of structural tensors, denoted as $\mathbf{x} \mapsto \mathsf{M}^{(\ell)}(\mathbf{x})$ for $\ell = 1, 2$, such that $\mathsf{M}^{(\ell)}(\mathbf{x}) := \mathbf{a}^{(\ell)}(\mathbf{x}) \otimes \mathbf{a}^{(\ell)}(\mathbf{x})$ [56,57]. More specifically, the strain energy function writes

$$\begin{aligned} w(\mathbf{x}, \mathsf{F}) = \mu_1(\mathbf{x}) \frac{\|\mathsf{F}\|^2}{(\det(\mathsf{F}))^{2/3}} + \mu_2(\mathbf{x}) \frac{\|\mathrm{Cof}(\mathsf{F})\|^3}{(\det(\mathsf{F}))^2} + \mu_3(\mathbf{x}) h(\det(\mathsf{F})) \\ + \frac{\mu_4(\mathbf{x})}{\beta_4} \sum_{\ell=1}^{2} \exp\left(\beta_4 \langle \|\mathsf{F}\mathbf{a}^{(\ell)}(\mathbf{x})\|^2 - 1 \rangle_m^2\right) - e(\mathbf{x}) \,, \end{aligned} \tag{5}$$

where $e(\mathbf{x}) = w(\mathbf{x}, \mathsf{I})$, $\langle g \rangle_m$ denotes the Macaulay Bracket (that is, $\langle g \rangle_m := \max(0, g)$) and $h :]0, +\infty[\to [0, +\infty[$ is the convex function defined as

$$h(\delta) := \delta^{\beta_3} + \delta^{-\beta_3} - 2 \,. \tag{6}$$

The first three terms in the right hand side of Eq. (5) represent an isochoric Mooney–Rivlin-like contribution, while the term with summation represents the anisotropic part in the strain energy function. In what follows, it is assumed that the material parameters are uniformly bounded from below by strictly positive real numbers, $\mu_j(\mathbf{x}) \geqslant \mu_j^{min} > 0$ for all $\mathbf{x}$ in $\mathscr{B}$, and that $\beta_3 > 2$ and $\beta_4 > 0$. It can then be shown that strain energy function defined by Eq. (5) satisfies the following fundamental properties.

1. *Polyconvexity.* The stored energy function w is polyconvex, meaning that there exists a convex function $w^\star(\mathbf{x}, \cdot, \cdot, \cdot) : \mathbb{M}_3 \times \mathbb{M}_3 \times]0, +\infty[\to \mathbb{R}$ such that $w(\mathbf{x}, \mathsf{F}) = w^\star(\mathbf{x}, \mathsf{F}, \mathrm{Cof}(\mathsf{F}), \det(\mathsf{F}))$ (the proof follows from standard arguments; see [54,58,59]). Moreover, it also satisfies the Legendre–Hadamard condition [52] (see also [43,53] for theoretical treatments).
2. *Coercivity.* The function $w^\star$ satisfies the coercivity inequality:

$$w^\star(\mathbf{x}, \mathsf{F}, \mathsf{H}, \delta) \geqslant k_0 \left(\|\mathsf{F}\|^p + \|\mathsf{H}\|^q + \delta^{\beta_3}\right) - k_1 \quad \forall\, \mathbf{x} \in \mathscr{B} \,, \tag{7}$$

wherein $k_0 > 0$, $k_1 \in \mathbb{R}$ and

$$\frac{3}{2} < p = \frac{6\beta_3}{3\beta_3 + 2} < 2 \,, \quad \frac{3}{2} < q = \frac{3\beta_3}{\beta_3 + 2} < 3 \,. \tag{8}$$

The two above properties (polyconvexity and coercivity) ensure the existence of at least one solution to the nonlinear boundary value problem [52,54].
3. *Elastic behavior at small strains.* The elasticity tensor $[\![C]\!]$ at small strains is given by

$$[\![C(\mathbf{x})]\!] = 6\mu_3(\mathbf{x})\beta_3^2 [\![J]\!] + \left(4\mu_1(\mathbf{x}) + 6\sqrt{3}\mu_2(\mathbf{x})\right)[\![K]\!] + 8\mu_4(\mathbf{x}) \sum_{\ell=1}^{2} \mathbb{1}_{\mathcal{S}_\ell}(\mathsf{E}) \mathsf{M}^{(\ell)} \otimes \mathsf{M}^{(\ell)} \,, \tag{9}$$

where $\mathcal{S}_\ell$ denotes the set of deformation tensors E such that $\mathrm{Tr}(\mathsf{E}\mathsf{M}^{(\ell)}) > 0$, $[\![J]\!]$ and $[\![K]\!]$ are the following fourth-order projectors:

$$[\![J]\!] := \frac{1}{3} \mathsf{I} \otimes \mathsf{I} \,, \quad [\![K]\!] := [\![I]\!] - [\![J]\!] \,, \tag{10}$$

with $[\![I]\!]$ the identity tensor of fourth rank. Eq. (9) shows that the hyperelastic material exhibits an isotropic behavior at small strains, with the bulk and shear moduli respectively defined as $2\mu_3(\mathbf{x})\beta_3^2$ and $2\mu_1(\mathbf{x}) + 3^{3/2}\mu_2(\mathbf{x})$, whenever compression is undergone along the two directions defined by $\mathbf{a}^{(1)}(\mathbf{x})$ and $\mathbf{a}^{(2)}(\mathbf{x})$. When a local stretch is prescribed along the direction defined by, say $\mathbf{a}^{(1)}(\mathbf{x})$, then the elasticity tensor exhibits transverse isotropy with respect to $\mathbf{a}^{(1)}(\mathbf{x})$ (see [48]). Apart from these two situations, the elastic behavior at small strains turns out to be anisotropic.

3. Construction of a random field model

3.1. Methodological aspects

Let $\{W_\varepsilon(\mathbf{x},\mathsf{F}),(\mathbf{x},\mathsf{F})\in\mathscr{B}\times\mathbb{M}_3^+\}$ be the strain energy function random field (defined on a given probability space) corresponding to the probabilistic modeling of the strain energy function $w:\mathscr{B}\times\mathbb{M}_3^+\to\mathbb{R}$ introduced in the previous section. In order to algebraically ensure the well-posedness of the nonlinear boundary value problem (see [23] for a discussion focusing on elliptic boundary value problems), the following ε-regularization is introduced:

$$W_\varepsilon(\mathbf{x},\mathsf{F}) := \frac{1}{1+\varepsilon}\left(W(\mathbf{x},\mathsf{F})+\varepsilon\,\mathbb{E}\{W(\mathbf{x},\mathsf{F})\}\right)\,, \tag{11}$$

where $0<\varepsilon\ll 1$ is the regularizing parameter (the value of which can be arbitrarily chosen, e.g. $\varepsilon=10^{-6}$) and $\{W(\mathbf{x},\mathsf{F}),(\mathbf{x},\mathsf{F})\in\mathscr{B}\times\mathbb{M}_3^+\}$ is the random field such that

$$\begin{aligned} W(\mathbf{x},\mathsf{F}) = {} & G_1(\mathbf{x})\frac{\|\mathsf{F}\|^2}{(\det(\mathsf{F}))^{2/3}}+G_2(\mathbf{x})\frac{\|\mathrm{Cof}(\mathsf{F})\|^3}{(\det(\mathsf{F}))^2}+G_3(\mathbf{x})h(\det(\mathsf{F}))\\ & +\frac{G_4(\mathbf{x})}{\beta_4}\sum_{\ell=1}^{2}\exp\left(\beta_4\langle\|\mathsf{F}\,\mathbf{a}^{(\ell)}(\mathbf{x})\|^2-1\rangle_m^2\right)-E(\mathbf{x})\,, \end{aligned} \tag{12}$$

where $E(\mathbf{x})=W(\mathbf{x},\mathsf{I})$ and h is the convex function defined by Eq. (6). In Eq. (12), $\{\mathbf{G}(\mathbf{x})=(G_1(\mathbf{x}),\ldots,G_4(\mathbf{x})),\mathbf{x}\in\mathscr{B}\}$ is the random field with values in $(\mathbb{R}_+^*)^4$ associated with the randomization of the material parameters, and the parameters $\beta_3>2$ and $\beta_4>0$ are kept deterministic in the present framework (whenever necessary, these two parameters can be made random as well). Moreover, it is assumed that the mean function $\mathbf{x}\mapsto\mathbb{E}\{\mathbf{G}(\mathbf{x})\}$ of $\{\mathbf{G}(\mathbf{x}),\mathbf{x}\in\mathscr{B}\}$ is homogeneous over $\mathscr{B}$, that is $\mathbb{E}\{\mathbf{G}(\mathbf{x})\}=\underline{\mathbf{g}}=(\underline{g}_1,\ldots,\underline{g}_4)$ for any $\mathbf{x}$ in $\mathscr{B}$, and such that the mean strain energy function $\mathbf{x}\mapsto\mathbb{E}\{W(\mathbf{x},\mathsf{F})\}$ satisfies a uniform coercivity property. Following this construction, and upon substituting Eq. (12) in Eq. (11), the strain energy function $W_\varepsilon(\mathbf{x},\mathsf{F})$ reads as

$$\begin{aligned} W_\varepsilon(\mathbf{x},\mathsf{F}) = {} & G_{\varepsilon,1}(\mathbf{x})\frac{\|\mathsf{F}\|^2}{(\det(\mathsf{F}))^{2/3}}+G_{\varepsilon,2}(\mathbf{x})\frac{\|\mathrm{Cof}(\mathsf{F})\|^3}{(\det(\mathsf{F}))^2}+G_{\varepsilon,3}(\mathbf{x})h(\det(\mathsf{F}))\\ & +\frac{G_{\varepsilon,4}(\mathbf{x})}{\beta_4}\sum_{\ell=1}^{2}\exp\left(\beta_4\langle\|\mathsf{F}\,\mathbf{a}^{(\ell)}(\mathbf{x})\|^2-1\rangle_m^2\right)-E(\mathbf{x})\,, \end{aligned} \tag{13}$$

where $G_{\varepsilon,j}(\mathbf{x})$, $1\leqslant j\leqslant 4$, can be identified as

$$G_{\varepsilon,j}(\mathbf{x})=\frac{1}{1+\varepsilon}(G_j(\mathbf{x})+\varepsilon\,\underline{g}_j)\,. \tag{14}$$

Furthermore, it follows that

$$G_{\varepsilon,j}(\mathbf{x})\geqslant\mu_j^{min}>0 \tag{15}$$

almost surely, $\forall\,\mathbf{x}\in\mathscr{B}$, with

$$\mu_j^{min}=\frac{\varepsilon}{1+\varepsilon}\,\underline{g}_j\,. \tag{16}$$

Following the discussion in Section 2.2, Eq. (15) then implies that the stochastic nonlinear boundary value problem is well posed, and serves as an a posteriori motivation to resort on the regularized functional defined in Eq. (12). In addition, the elasticity tensor random field $\{[\![\mathbf{C}_\varepsilon(\mathbf{x})]\!],\mathbf{x}\in\mathscr{B}\}$ associated with the regularized strain energy function can be obtained through a classical linearization procedure (see e.g. [58]) and is given by

$$[\![\mathbf{C}_\varepsilon(\mathbf{x})]\!]=\frac{1}{1+\varepsilon}\left([\![\mathbf{C}(\mathbf{x})]\!]+\varepsilon\,[\![\underline{C}(\mathbf{x})]\!]\right)\,, \tag{17}$$

in which $[\![\mathbf{C}(\mathbf{x})]\!]$ and the mean value $[\![\underline{C}(\mathbf{x})]\!]:=\mathbb{E}\{[\![\mathbf{C}(\mathbf{x})]\!]\}$ are defined, by identification, as

$$[\![\mathbf{C}(\mathbf{x})]\!]=\underbrace{6G_3(\mathbf{x})\beta_3^2[\![J]\!]+\left(4G_1(\mathbf{x})+6\sqrt{3}G_2(\mathbf{x})\right)[\![K]\!]}_{\text{Isotropic contribution}}+\underbrace{8G_4(\mathbf{x})\sum_{\ell=1}^{2}\mathbb{1}_{\mathcal{S}_\ell}(\mathsf{E})\mathsf{M}^{(\ell)}\otimes\mathsf{M}^{(\ell)}}_{\text{Anisotropic contribution}} \tag{18}$$

and

$$[\![\underline{C}(\mathbf{x})]\!] = \underbrace{6\underline{g}_3\beta_3^2[\![J]\!] + \left(4\underline{g}_1 + 6\sqrt{3}\underline{g}_2\right)[\![K]\!]}_{\text{Isotropic contribution}} + \underbrace{8\underline{g}_4 \sum_{\ell=1}^{2} \mathbb{1}_{\mathcal{S}_\ell}(\mathsf{E}(\mathbf{x}))\mathsf{M}^{(\ell)}(\mathbf{x}) \otimes \mathsf{M}^{(\ell)}(\mathbf{x})}_{\text{Anisotropic contribution}} . \tag{19}$$

It should be noticed that while the mean function of $\{\mathbf{G}(\mathbf{x}), \mathbf{x} \in \mathscr{B}\}$ is chosen as independent of the spatial location, the mean function of the elasticity tensor is, in general, spatially-dependent due to the presence of the indicator function $\mathbf{x} \mapsto \mathbb{1}_{\mathcal{S}_\ell}(\mathsf{E}(\mathbf{x}))$. By construction, the mean function $\mathbf{x} \mapsto [\![\underline{C}(\mathbf{x})]\!]$ is such that the linearized elasticity problem is well posed, and the form defined by Eq. (17) subsequently ensures that the random bilinear form involved in the stochastic linearized boundary value problem is uniformly elliptic (see [25] for a discussion). By definition, the isotropic part of $[\![\mathbf{C}_\varepsilon(\mathbf{x})]\!]$ can be written as

$$3C_{\varepsilon,1}(\mathbf{x})[\![J]\!] + 2C_{\varepsilon,2}(\mathbf{x})[\![J]\!] , \tag{20}$$

where $C_{\varepsilon,1}(\mathbf{x})$ and $C_{\varepsilon,2}(\mathbf{x})$ are the regularized bulk and shear moduli, and $[\![J]\!]$ and $[\![K]\!]$ are the tensors defined in Eq. (10). Summing up the isotropic contributions in Eqs. (18) and (19), and taking into account Eq. (14), it follows from Eq. (20) that

$$C_{\varepsilon,1}(\mathbf{x}) = 2\beta_3^2 G_{\varepsilon,3}(\mathbf{x}) \tag{21}$$

and

$$C_{\varepsilon,2}(\mathbf{x}) = 2G_{\varepsilon,1}(\mathbf{x}) + 3\sqrt{3}G_{\varepsilon,2}(\mathbf{x}) . \tag{22}$$

Similarly, the isotropic part of $[\![\mathbf{C}(\mathbf{x})]\!]$ is given by $3C_1(\mathbf{x})[\![J]\!] + 2C_2(\mathbf{x})[\![K]\!]$, with $C_1(\mathbf{x}) = 2\beta_3^2 G_3(\mathbf{x}) > 0$ and $C_2(\mathbf{x}) = 2G_1(\mathbf{x}) + 3\sqrt{3}G_2(\mathbf{x}) > 0$. The consistency at small strains then implies that

$$G_3(\mathbf{x}) = \frac{C_1(\mathbf{x})}{2\beta_3^2} , \quad G_2(\mathbf{x}) = 3^{-3/2}\left(C_2(\mathbf{x}) - 2G_1(\mathbf{x})\right) , \tag{23}$$

and does not involve parameter $G_4(\mathbf{x})$. The above equation allows a more convenient representation of the stochastic strain energy function to be introduced. To this aim, note that a normalized random variable $U_1(\mathbf{x})$, with values in $]0, 1[$, can be defined such that

$$2G_1(\mathbf{x}) = C_2(\mathbf{x})U_1(\mathbf{x}) , \tag{24}$$

so that the random variable $G_2(\mathbf{x})$ can equivalently be written (see the second equation in Eq. (23)) as

$$G_2(\mathbf{x}) = 3^{-3/2}C_2(\mathbf{x})\left(1 - U_1(\mathbf{x})\right) . \tag{25}$$

Two strategies can be pursued at this stage.

- In a first modeling approach, the strain energy function is considered as a function of $\{\mathbf{G}(\mathbf{x}), \mathbf{x} \in \mathscr{B}\}$. In this case, the assumptions raised by the mathematical formulation do not introduce cross-related information among the variables, and the fields $\{G_i(\mathbf{x}), \mathbf{x} \in \mathscr{B}\}$ and $\{G_j(\mathbf{x}), \mathbf{x} \in \mathscr{B}\}$, $i \neq j$, would hence be statistically independent.
- In a second approach, the strain energy function is alternatively parametrized by the random fields $\{C_i(\mathbf{x}), \mathbf{x} \in \mathscr{B}\}$, $i = 1, 2$, $\{U_1(\mathbf{x}), \mathbf{x} \in \mathscr{B}\}$ and $\{G_4(\mathbf{x}), \mathbf{x} \in \mathscr{B}\}$. Here, the consistency at small strains (see Eqs. (24)–(25)) raises relations that generate statistical dependencies in the variables defining $W(\mathbf{x}, \mathsf{F})$, and the fields $\{G_1(\mathbf{x}), \mathbf{x} \in \mathscr{B}\}$, $\{G_2(\mathbf{x}), \mathbf{x} \in \mathscr{B}\}$ and $\{G_3(\mathbf{x}), \mathbf{x} \in \mathscr{B}\}$ are defined in terms of the aforementioned random fields using the one-to-one mappings given by Eqs. (24), (25) and the first equation in (23).

Clearly, the former strategy turns out to be easier to handle in terms of both technical derivations and sampling issues. The latter choice raises, by contrast, more complex calculations, but offers the benefit of relying, at least in part, on information at small strains. This property may be found useful, especially for identification issues, and motivates the selection of this approach hereinafter. Let then $\{\mathbf{P}(\mathbf{x}) := (C_1(\mathbf{x}), C_2(\mathbf{x}), U_1(\mathbf{x}), G_4(\mathbf{x})), \mathbf{x} \in \mathscr{B}\}$ be the vector-valued random field of model parameters. Following the standard approach to the modeling of non-Gaussian processes, the random field is defined through the memoryless transformation

$$\mathbf{P}(\mathbf{x}) := \mathscr{H}(\boldsymbol{\Xi}(\mathbf{x})) , \quad \forall\, \mathbf{x} \in \mathscr{B} , \tag{26}$$

where $\{\boldsymbol{\Xi}(\mathbf{x}) = (\Xi_1(\mathbf{x}), \ldots, \Xi_4(\mathbf{x})), \mathbf{x} \in \mathbb{R}^3\}$ is a second-order centered Gaussian random field defined by the covariance function (which may be inferred either from measurements or expertise)

$$\mathsf{R}_{\boldsymbol{\Xi}}(\mathbf{x}, \mathbf{y}) = \mathbb{E}\{\boldsymbol{\Xi}(\mathbf{x}) \otimes \boldsymbol{\Xi}(\mathbf{y})\} := \mathrm{diag}(R_1(\mathbf{x}, \mathbf{y}), \ldots, R_4(\mathbf{x}, \mathbf{y})) \,, \tag{27}$$

where $\mathsf{R}_{\boldsymbol{\Xi}}(\mathbf{x}, \mathbf{x}) = \mathsf{I}$ and $(\mathbf{x}, \mathbf{y}) \mapsto R_i(\mathbf{x}, \mathbf{y})$ denotes the correlation function of the real-valued Gaussian random field $\{\Xi_i(\mathbf{x}), \mathbf{x} \in \mathbb{R}^3\}$. Eq. (27) implies that the random fields $\{\Xi_j(\mathbf{x}), \mathbf{x} \in \Omega\}$ and $\{\Xi_k(\mathbf{x}), \mathbf{x} \in \Omega\}$, $j \neq k$, are statistically independent from one another. In this work, the nonlinear transformation $\mathscr{H}$ is obtained by constructing the first-order marginal probability distribution of $\{\mathbf{P}(\mathbf{x}), \mathbf{x} \in \mathscr{B}\}$, or equivalently of the stored energy function random field. Here, this distribution is chosen as independent of $\mathbf{x}$ in order to simplify exposure, and spatial dependencies can be considered in a straightforward manner. Once the correlation function $\mathsf{R}_{\boldsymbol{\Xi}}(\mathbf{x}, \mathbf{y})$ associated with the underlying vector-valued Gaussian field $\{\boldsymbol{\Xi}(\mathbf{x}), \mathbf{x} \in \mathbb{R}^3\}$ and mapping $\mathscr{H}$ are specified, Eq. (26) completely defines the system of marginal probability distributions for the random field $\{\mathbf{P}(\mathbf{x}), \mathbf{x} \in \mathscr{B}\}$. The construction of $\mathscr{H}$ is specifically addressed in the next section.

Remark 3.1. The selection of $G_2(\mathbf{x})$ as an independent variable in the consistency relations is irrelevant, since similar expressions would be obtained by choosing $G_1(\mathbf{x})$ in lieu of $G_2(\mathbf{x})$. More specifically, one shall first extract $G_1(\mathbf{x})$ as

$$G_1(\mathbf{x}) = \frac{1}{2}\left(C_2(\mathbf{x}) - 3^{3/2} G_2(\mathbf{x})\right) \,, \tag{28}$$

and upon introducing the random variable $U_2(\mathbf{x})$ such that $C_2(\mathbf{x})U_2(\mathbf{x}) = 3^{3/2}G_2(\mathbf{x})$, it is seen that

$$2G_1(\mathbf{x}) = C_2(\mathbf{x})(1 - U_2(\mathbf{x})) \,. \tag{29}$$

The similitude in the expressions thus obtained follows by comparing Eq. (29) with Eq. (25).

3.2. Information-theoretic formulation

As previously indicated, the mapping $\mathscr{H}$ is defined by constructing the first-order marginal probability distribution of the random field $\{\mathbf{P}(\mathbf{x}), \mathbf{x} \in \mathscr{B}\}$, which corresponds to the probability distribution of the vector-valued random variable $\mathbf{P}(\mathbf{x})$, $\mathbf{x}$ being fixed in $\mathscr{B}$. Based on the previous section, minimal requirements include that $C_1(\mathbf{x})$, $C_2(\mathbf{x})$ and $G_4(\mathbf{x})$ are strictly positive almost surely, and that $0 < U_1(\mathbf{x}) < 1$ almost surely. Additionally, it is assumed that the mean values of random variables $C_1(\mathbf{x})$, $C_2(\mathbf{x})$ and $G_4(\mathbf{x})$ are known. From a probabilistic point of view, the former constraints can be accounted for by generating repulsive terms in the probability law. As demonstrated in [60], this can be achieved by imposing the following constraint:

$$\mathbb{E}\{\log(P_j(\mathbf{x}))\} = \varpi_j \,, \quad |\varpi_j| < +\infty \,, \quad j = 1, 2, \tag{30a}$$
$$\mathbb{E}\{\log(P_3(\mathbf{x}))\} = \zeta_1 \,, \quad |\zeta_1| < +\infty \,, \tag{30b}$$
$$\mathbb{E}\{\log(1 - P_3(\mathbf{x}))\} = \zeta_2 \,, \quad |\zeta_2| < +\infty \,, \tag{30c}$$
$$\mathbb{E}\{\log(P_4(\mathbf{x}))\} = \varsigma_4 \,, \quad |\varsigma_4| < +\infty \,, \tag{30d}$$

where it is recalled that $P_1(\mathbf{x}) = C_1(\mathbf{x})$, $P_2(\mathbf{x}) = C_2(\mathbf{x})$, $P_3(\mathbf{x}) = U_1(\mathbf{x})$ and $P_4(\mathbf{x}) = G_4(\mathbf{x})$ by convention. The latter constraints related the mean values take the natural form

$$\mathbb{E}\{P_j(\mathbf{x})\} = \underline{c}_j \,, \quad j = 1, 2 \,, \tag{31a}$$
$$\mathbb{E}\{P_4(\mathbf{x})\} = \underline{g}_4 \,. \tag{31b}$$

It should be noticed that the properties $G_1(\mathbf{x}) > 0$ and $G_2(\mathbf{x}) > 0$ (almost surely) readily follow, by construction (see Eqs. (24) and (25)). The probability density function $f_{\mathbf{P}(\mathbf{x})}$ defining $\mathbf{P}(\mathbf{x})$, with support $\mathcal{S}_{\mathbf{P}}$, is next constructed by invoking the framework of information theory [61,62]. Within this framework, the most objective choice for $f_{\mathbf{P}(\mathbf{x})}$ is obtained by maximizing Shannon's differential entropy [63], which writes

$$\mathscr{E}(f) = -\int_{\mathcal{S}_{\mathbf{P}}} f(\mathbf{z}) \log(f(\mathbf{z}))\, d\mathbf{z} \tag{32}$$

for any probability density function f supported over $\mathcal{S}_{\mathbf{P}} \subset \mathbb{R}^4$ (with $d\mathbf{z}$ the Lebesgue measure on $\mathbb{R}^4$), under the aforementioned set of constraints (defined by Eqs. (30a)–(31b)). In practice, this functional optimization problem is solved by proceeding to the calculus of variation on the associated Lagrangian, and the solution reads in the present case as

$$f_{\mathbf{P}(\mathbf{x})}(\mathbf{p}) = \mathbb{1}_{\mathcal{S}_{\mathbf{P}}}(\mathbf{p}) c_0 \exp\{-\Upsilon(\mathbf{p})\} , \tag{33}$$

where c_0 is the normalization constant and the function Υ is defined as

$$\begin{aligned}\Upsilon(\mathbf{p}) = &\underbrace{\lambda_1^{(1)} p_1 + \lambda_2^{(1)} \log(p_1)}_{\substack{\text{Information on } P_1(\mathbf{x}) \\ \text{(see Eqs. (30a)–(31a))}}} + \underbrace{\lambda_1^{(2)} p_2 + \lambda_2^{(2)} \log(p_2)}_{\substack{\text{Information on } P_2(\mathbf{x}) \\ \text{(see Eqs. (30a)–(31a))}}} \\ &+ \underbrace{\lambda_1^{(3)} \log(p_3) + \lambda_2^{(3)} \log(1-p_3)}_{\substack{\text{Information on } P_3(\mathbf{x}) \\ \text{(see Eqs. (30b)–(30c))}}} + \underbrace{\lambda_1^{(4)} p_4 + \lambda_2^{(4)} \log(p_4)}_{\substack{\text{Information on } P_4(\mathbf{x}) \\ \text{(see Eqs. (30d)–(31b))}}} .\end{aligned} \tag{34}$$

In Eq. (34), $\lambda_1^{(i)}$ and $\lambda_2^{(i)}$ are Lagrange multipliers associated with variable $P_i(\mathbf{x})$, and the set of multipliers is such that $f_{\mathbf{P}(\mathbf{x})}$ is integrable over $\mathbb{R}^4$. Since the indicator function $\mathbb{1}_{\mathcal{S}_{\mathbf{P}}}$ is separable in the present case, Eqs. (33) and (34) show that $f_{\mathbf{P}(\mathbf{x})}$ has also a separable structure, so that the random variables $P_1(\mathbf{x})$, $P_2(\mathbf{x})$, $U_1(\mathbf{x})$ and $G_4(\mathbf{x})$ ($\mathbf{x}$ being fixed in Ω) are statistically independent. Moreover, and upon performing a change of variables between the Lagrange multipliers and the hyperparameters associated with labeled statistical distributions, it can be deduced that:

- For $j \in \{1, 2\}$, the parameter $P_j(\mathbf{x})$ follows a Gamma distribution with shape and scale parameters defined by $\delta_{C_j}^{-2}$ and $\underline{c}_j \delta_{C_j}^2$ (with $\underline{c}_j$ and δ_{C_j} the mean and coefficient of variation of $C_j(\mathbf{x})$).
- The random variable $U_1(\mathbf{x})$ is distributed according to a Beta distribution, with parameters $(\mathcal{U}_1, \mathcal{U}_2)$. Denoting by δ_{U_1} the coefficient of variation of $U_1(\mathbf{x})$, one has:

$$\underline{u}_1 := \mathbb{E}\{U_1\} = \frac{\mathcal{U}_1}{\mathcal{U}_1 + \mathcal{U}_2} , \quad \delta_{U_1}^2 = \frac{\mathcal{U}_2}{\mathcal{U}_1(1 + \mathcal{U}_1 + \mathcal{U}_2)} . \tag{35}$$

- The parameter $G_4(\mathbf{x})$ also follows a Gamma distribution with shape and scale parameters defined by $\delta_{G_4}^{-2}$ and $\underline{g}_4 \delta_{G_4}^2$ (with similar notations).

It then follows that the non-Gaussian random fields of interest can be defined as follows:

$$C_j(\mathbf{x}) := (\mathfrak{G}_{k_j,\theta_j}^{-1} \circ \Phi)(\Xi_j(\mathbf{x})) , \quad k_j = \delta_{C_j}^{-2} , \quad \theta_j = \underline{c}_j \delta_{C_j}^2 , \quad j \in \{1, 2\} , \tag{36a}$$

$$U_1(\mathbf{x}) := (\mathfrak{B}_{\mathcal{U}_1,\mathcal{U}_2}^{-1} \circ \Phi)(\Xi_3(\mathbf{x})) , \tag{36b}$$

$$G_4(\mathbf{x}) := (\mathfrak{G}_{k_4,\theta_4}^{-1} \circ \Phi)(\Xi_4(\mathbf{x})) , \quad k_4 = \delta_{G_4}^{-2} , \quad \theta_4 = \underline{g}_4 \delta_{G_4}^2 , \tag{36c}$$

where $\mathfrak{G}_{k,\theta}^{-1}$ is the inverse cumulative distribution function of the Gamma distribution with shape parameter k and scale parameter θ, $\mathfrak{B}_{s_1,s_2}^{-1}$ is inverse cumulative distribution function of the Beta distribution with parameters (s_1, s_2), and Φ is the cumulative distribution function of the standard normal distribution. The nonlinear transformation $\mathscr{H}$ introduced in Eq. (26) is thus completely defined by Eq. (36), and the strain energy function random field is finally defined by combining Eqs. (23)–(25) with Eqs. (12)–(14). By construction, the random fields $\{P_1(\mathbf{x}), \mathbf{x} \in \mathscr{B}\}$, $\{P_2(\mathbf{x}), \mathbf{x} \in \mathscr{B}\}$, $\{U_1(\mathbf{x}), \mathbf{x} \in \mathscr{B}\}$, and $\{G_4(\mathbf{x}), \mathbf{x} \in \mathscr{B}\}$ are statistically independent. However, it is a noticeable effect of the construction that the random fields $\{G_1(\mathbf{x}), \mathbf{x} \in \mathscr{B}\}$ and $\{G_2(\mathbf{x}), \mathbf{x} \in \mathscr{B}\}$ end up being dependent, following Eqs. (24) and (25). By contrast, the random fields $\{G_3(\mathbf{x}), \mathbf{x} \in \mathscr{B}\}$ and $\{G_4(\mathbf{x}), \mathbf{x} \in \mathscr{B}\}$ remain statistically independent from all other random fields. It should also be noticed that the aforementioned hyperparameters become spatially-dependent whenever the terms in the right-hand sides of the constraint equations (considered while maximizing the entropy) depend on spatial location—in which case the family of first-order marginal probability laws, indexed by $\mathscr{B}$, can be constructed through the proposed approach. In the next section, a sampling algorithm for the proposed random field model is presented.

4. Sampling the random field model on manifolds

Within the proposed framework, realizations of the strain energy function random field can be obtained by combining realizations of the Gaussian random field $\{\boldsymbol{\Xi}(\mathbf{x}), \mathbf{x} \in \mathscr{B}\}$ and Eqs. (26), (12) and (14). When the domain

$\mathscr{B}$ is homotopic to a simple (simplified) geometry, typically a sphere, covariance models (satisfying potentially some symmetry or periodicity properties) for the Gaussian fields $\{\Xi_j(\mathbf{x}), \mathbf{x} \in \mathscr{B}\}$, $1 \leqslant j \leqslant 4$, can be easily constructed, inferred from experiments or selected in suitable (e.g. Matérn-type) classes of covariance kernels. Standard sampling techniques, including direct or iterative factorization methods [64] and spectral approaches [65], can subsequently be applied in order to generate independent realizations of the field.

In this work, we focus on the more intricate situation where the domain $\mathscr{B}$ is not homotopic to a sphere and involves boundaries defined by arbitrary smooth manifolds. In order to tackle this challenging issue, and following [66], our approach relies on defining each random field $\{\Xi_j(\mathbf{x}), \mathbf{x} \in \mathscr{B}\}$ as the solution (see [67,68]) of the spatial stochastic partial differential equation (SPDE)

$$\left[\gamma^2(\mathbf{x}) - \langle \boldsymbol{\nabla}, \mathsf{H}(\mathbf{x})\boldsymbol{\nabla}\rangle_{\mathbb{R}^3}\right]^{\zeta/2} \Xi_j(\mathbf{x}) = \dot{\mathscr{W}}(\mathbf{x}) \,, \quad \mathbf{x} \in \mathscr{B} \,, \tag{37}$$

where $\gamma(\mathbf{x}) > 0$ is parameter controlling the correlation range, $\mathsf{H}(\mathbf{x})$ is the positive-definite diffusion matrix, $\zeta \in \mathbb{N}_*^+$ and $\{\mathscr{W}(\mathbf{x}), \mathbf{x} \in \mathscr{B}\}$ is the spatial normalized Gaussian white noise. In three-dimensional applications, the integer ζ satisfies the equality $\zeta = \nu + 3/2$, where $\nu > 0$ controls the smoothness of the solution. When the above SPDE is analytically solved over $\mathbb{R}^3$, the complete class of Matérn covariance kernels (which include the widely-used exponential and square-exponential kernels) can be recovered, and the solution field can be shown to be $\lfloor \nu - 1 \rfloor$ differentiable. It should be noticed that other types of (e.g. oscillating) covariance functions can also be considered by using nested SPDEs, as discussed in [66,69]. The definition of the diffusion field $\mathbf{x} \mapsto \mathsf{H}(\mathbf{x})$ is a key ingredient of the proposed methodology, since it allows an ad-hoc covariance structure to be defined, albeit in a non-explicit form, on the complex geometry of interest. This can be achieved, for instance, by selecting a diagonal form for the field $\mathbf{x} \mapsto \mathsf{H}(\mathbf{x})$:

$$\mathsf{H}(\mathbf{x}) := \sum_{i=1}^{3} \hat{\tau}_i \, \hat{\mathbf{e}}^{(i)}(\mathbf{x}) \otimes \hat{\mathbf{e}}^{(i)}(\mathbf{x}) \quad \forall \, \mathbf{x} \in \mathscr{B} \,, \tag{38}$$

where $\{\hat{\mathbf{e}}^{(i)}(\mathbf{x})\}_{i=1}^3$ is a local basis that can capture, for instance, the features of the considered geometry and $\{\hat{\tau}_i\}_{i=1}^3$ is a set of strictly positive parameters controlling the magnitude of the local anisotropy. Illustrative two-dimensional examples can be found in [67,68] for stationary and non-stationary cases, and a detailed application of this strategy to vascular vessels is presented in Section 5.

In this paper, the value $\nu = 1/2$ is selected (hence, $\zeta = 2$), so that a classical Galerkin method can be used to solve Eq. (37) with homogeneous Neumann boundary conditions. By assuming that the discretization of the domain $\mathscr{B}$ involves n_d nodes, the stochastic weak solution of the SPDE is then expanded as follows

$$\Xi_j(\mathbf{x}) \approx \sum_{i=1}^{n_d} \eta_i \psi_i(\mathbf{x}) \tag{39}$$

where $\{\psi_i\}_{i=1}^n$ is the finite element basis consisting of piece-wise linear functions. It can then be shown that the weights $\eta_1, \ldots, \eta_{n_d}$ are distributed according to a Gaussian distribution and such that the random vector $\boldsymbol{\eta} := (\eta_1, \ldots, \eta_{n_d})$ is centered and exhibits a covariance matrix denoted by Q^{-1}, where Q is the precision matrix defined as

$$\mathsf{Q} := (\mathcal{M} + \mathcal{K})^{\mathrm{T}} \mathcal{N}^{-1} (\mathcal{M} + \mathcal{K}) \,. \tag{40}$$

In the equation above, the $(n_d \times n_d)$ matrices $\mathcal{M}$, $\mathcal{K}$ and $\mathcal{N}$ are defined component-wise as

$$\mathcal{M}_{ij} := \int_{\mathscr{B}} \gamma^2(\mathbf{x}) \psi_i(\mathbf{x}) \psi_j(\mathbf{x}) \, \mathrm{d}\mathbf{x} \,, \quad \mathcal{K}_{ij} := \int_{\mathscr{B}} \langle \boldsymbol{\nabla} \psi_i(\mathbf{x}), \mathsf{H}(\mathbf{x}) \boldsymbol{\nabla} \psi_j(\mathbf{x}) \rangle_{\mathbb{R}^3} \, \mathrm{d}\mathbf{x} \tag{41}$$

for $1 \leqslant i, j \leqslant n_d$ and

$$\mathcal{N}_{ij} := \int_{\mathscr{B}} \psi_i(\mathbf{x}) \psi_j(\mathbf{x}) \, \mathrm{d}\mathbf{x} \,. \tag{42}$$

Due to the structure of the right-hand side in Eq. (40), the precision matrix Q turns out to be full and consequently, the computation of its Cholesky factorization may be very time-consuming. In order to circumvent this drawback, one may alternatively consider the following sparse approximation (see [66] for a discussion):

$$\mathsf{Q} \approx (\mathcal{M} + \mathcal{K})^{\mathrm{T}} \mathcal{N}_d^{-1} (\mathcal{M} + \mathcal{K}) \,, \tag{43}$$

in which $\mathcal{N}_d$ is the diagonal matrix with entries $(\mathcal{N}_d)_{ii} := \sum_{j=1}^{n_d} \mathcal{N}_{ij}$, $1 \leqslant i \leqslant n_d$. In practice, realizations of $\{\Xi_j(\mathbf{x}), \mathbf{x} \in \mathscr{B}\}$ are then obtained by sampling the random vector $\boldsymbol{\eta}$ according to the centered Gaussian law with covariance matrix Q^{-1}, with Q defined either by Eq. (40) or (43) [93], and by using Eq. (39).

A few comments regarding the pros and cons of the aforementioned method are relevant at this point. First of all, the stochastic solver for the SPDE involves a finite element mesh which may coincide with the mesh related to the nonlinear mechanical problem, hence allowing for substantial computational savings when complex geometries are under consideration. Moreover, such a sampling strategy does not involve the storage of the full covariance matrix and can thus accommodate very large and dense meshes. Since the precision matrix is, by construction, sparse, fast factorization techniques can also be employed while sampling the random vector $\boldsymbol{\eta}$. Regarding disadvantages, one may first notice that the analytical form of the covariance kernel is unknown for bounded domains and/or spatially-dependent parameters fields. Furthermore, and as reported in [66–68], variance fluctuations may be observed while solving the SPDE on bounded domains or when heterogeneous diffusion fields are involved. In this case, the solution must be subsequently rescaled in order to ensure a zero mean and unit variance—which may increase the computational cost. Finally, the sparse inverse approximation $\mathcal{N}^{-1}$ of the matrix $\mathcal{N}$ can be shown to be singular for piecewise quadratic interpolations in two- and three-dimensional applications, so that other non-singular sparse inverse approximation for $\mathcal{N}^{-1}$ must be introduced in this case.

5. Uncertainty quantification in mechanics of arterial walls

This section is concerned with uncertainty modeling and propagation for soft biological tissues [41], with a specific emphasis on the mechanics of vascular vessels [46]. The latter are very prone to uncertainties raised by various sources including age, gender, and health state (see e.g. [70,71] for experimental evidences). For applications where the constitutive model of the wall plays an important role (e.g. in the computational study of atherosclerosis evolution [72] and failure for vascular grafts, for which compliance mismatch was reported to generate postoperative complications [73,74]; see [75] for a complementary discussion), such intrinsic variability must then be accounted for in numerical simulations. Although arterial walls are typically seen as a three-layer structure, with each layer being composed of an isotropic ground matrix reinforced by families of collagen fibers, the analysis is presently restricted, for illustration purposes, to the modeling of the intermediate layer, named the media. In this work, Monte Carlo simulations are used as the stochastic solver (note that discussions regarding the design of efficient stochastic solvers for nonlinear computational models are outside the scope of this paper; see [42] for a broad survey on uncertainty propagation), and the nonlinear boundary value problem is solved with the finite element method and a total Lagrangian formulation [76,77]; see [78,79] for a discussion about advanced techniques for the numerical modeling of arterial walls. In order to circumvent the well-known locking phenomenon raised by quasi-incompressibility, a three-field formulation with static condensation (mean dilatation method) is considered [80–82]. More specifically, a $\mathbb{P}_2$–$\mathbb{P}_0$–$\mathbb{P}_0$ discretization is used, and the displacement-based formulation is solved with a standard Newton–Raphson algorithm. The parallel finite element solver was implemented within Sandia's C++ Trilinos packages [83,84], and validated by using numerical benchmarks provided elsewhere.

The reminder of this section is organized as follows. In Section 5.1, the particular case of a homogeneous media strip under tension is first considered. Here, forward simulations are performed in order to get an insight about the influence of model hyperparameters on the variability of the stress response. In Section 5.2, heterogeneous media strips are next considered to investigate the impact of the correlation structure. Finally, an application to an arterial wall defined by a patient-specific geometry is presented in Section 5.3.

5.1. Case of homogeneous strips

As a first illustration, a homogeneous media strip undergoing a simple tensile test is considered. In this particular case, where only random variables (and not random fields) are involved, the stochastic parameters are easily sampled by using standard algorithms for univariate probability laws. It is assumed that the two preferred directions defining the anisotropic contributions in the stochastic strain energy function are defined as

$$\mathbf{a}^{(1)} = \cos(\theta)\mathbf{e}^{(1)} + \sin(\theta)\mathbf{e}^{(2)}\,, \quad \mathbf{a}^{(2)} = \cos(\theta)\mathbf{e}^{(1)} - \sin(\theta)\mathbf{e}^{(2)}\,, \tag{44}$$

where $\mathbf{e}^{(1)}$ and $\mathbf{e}^{(2)}$ span the median plane of the strip. The mean values of the random variables, the deterministic exponents β_3 and β_4 and the angle θ are identified by solving a least squares optimization problem where the

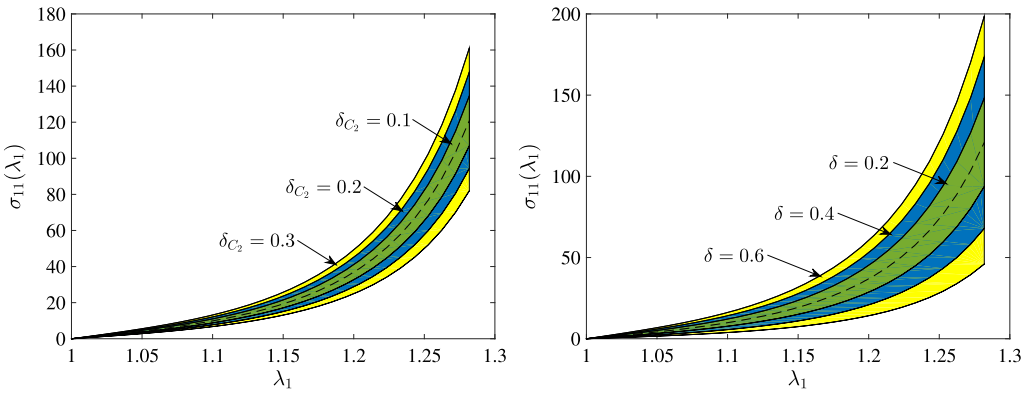

Fig. 1. Confidence regions (at a 90% probability level) of the Cauchy stress for a uniaxial tensile test. Left panel: $\delta_{C_1} = \delta_{G_4} = \delta_{U_1} = 0.1$, $\delta_{C_2} \in \{0.1, 0.2, 0.3\}$. Right panel: $\delta_{C_1} = \delta_{G_4} = \delta_{U_1} = \delta_{C_2} = \delta \in \{0.2, 0.4, 0.6\}$. The mean responses are represented in dashed lines.

relative error between the mean Cauchy stress and the experimental data provided in [85] is minimized. Here, a near incompressible solution is sought by adding a classical penalty term in the objective function. The obtained mean parameters are given by $\underline{g}_1 = 4.1543$, $\underline{g}_2 = 2.5084$, $\underline{g}_3 = 9.7227$ and $\underline{g}_4 = 19.285$ (in kPa). The values for the remaining deterministic parameters were obtained as $\beta_3 = 3.6537$, $\beta_4 = 500.02$ and $\theta = 46.274$ (degrees). By using the consistency relations with linearized elasticity, it is found that the mean values of the bulk and shear moduli are given by $\underline{c}_1 = 259.59$ and $\underline{c}_2 = 21.343$ (in kPa). Note that by combining Eqs. (23)–(25) with Eq. (35), the Lagrange multipliers associated with U_1 must satisfy the relations

$$\mathcal{U}_1 = \frac{2\underline{g}_1}{3^{3/2}\underline{g}_2}\mathcal{U}_2 \,, \quad \mathcal{U}_2 = \frac{1-\delta_{U_1}^2}{\eta(1+\eta)\delta_{U_1}^2} \,, \tag{45}$$

with $0 < \delta_{U_1} < 1$, hence leaving $\mathcal{U}_2$ as the only free hyperparameter in the probability distribution of U_1.

In order to illustrate the influence of the statistical fluctuations of the random variables, realizations of the stress response were computed by combining analytical derivations (for the components of the Cauchy stress tensor) with Monte Carlo simulations. The confidence interval at 90% is shown in Fig. 1 (left) for $\delta_{C_1} = \delta_{G_4} = \delta_{U_1} = 0.1$ and increasing values of the coefficient of variation for the random shear modulus C_2. As expected, it is observed that the confidence region becomes wider when δ_{C_2} increases. In order to facilitate interpretation, the evolution of the confidence region when the coefficients of variation of all input random variables are set to the same value and increased is also shown in Fig. 1 (right). In this case, all variables simultaneously exhibit larger fluctuations, hence making the variability much larger—even at contained stretches.

These results provide an assessment about the capability of the stochastic model associated with the first-order marginal probability law to faithfully reproduce variability in the stress response (as it is typically encountered, notably for soft biological tissues [41]), and are in accordance with previous results derived for isotropic hyperelastic materials [39,40].

5.2. Case of heterogeneous strips

In this second application, numerical simulations of tensile tests on heterogeneous media strips are carried out. Following the computational framework discussed in [47], media strips of length $l_{\text{strip}} = 10$ mm, width $w_{\text{strip}} = 3$ mm and thickness $t_{\text{stip}} = 0.5$ mm are considered. A displacement is prescribed at the top end of the specimens, while the bottom end is totally clamped. The mean parameters obtained in the previous Section 5.1 are retained as the mean values of the random field $\{\mathbf{G}(\mathbf{x}), \mathbf{x} \in \mathscr{B}\}$, and the preferred directions are given by Eq. (44). The SPDE approach described in Section 4 is used for sampling purposes, and the diffusion tensor is chosen as homogeneous over $\mathscr{B}$. The tensor H is then written as

$$\mathsf{H} := \kappa \mathsf{I} + \tau_1 \mathsf{M}^{(1)} + \tau_2 \mathsf{M}^{(2)} \,, \tag{46}$$

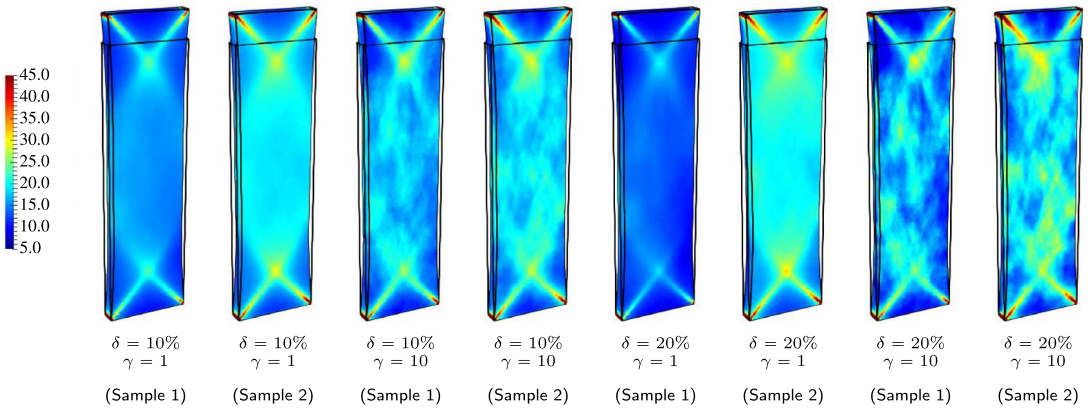

Fig. 2. Realizations of the Cauchy stress along the loading direction for several values of model hyperparameters.

Fig. 3. Meshed views of the patient-specific geometry (media) in its reference configuration.

regardless of the Gaussian field under consideration, with $\mathsf{M}^{(\ell)} = \mathbf{a}^{(\ell)} \otimes \mathbf{a}^{(\ell)}$, $\ell = 1, 2$. The parameters κ, τ_1 and τ_2 involved in Eq. (46) can be properly selected in order to adjust the anisotropy of the correlation structure inherited by the Gaussian random fields. The same coefficient of variation δ is considered for all the random fields and the remaining parameters κ, τ_1 and τ_2 are chosen as $\kappa = 0.1$ and $\tau_1 = \tau_2 = 10$. Realizations of the stress in the loading direction are shown in Fig. 2 for $\gamma \in \{1, 10\}$ and $\delta \in \{0.1, 0.2\}$.

This figure shows how the stochastic spatial fluctuations of the strain energy function impacts the local stress field. Moreover, it is seen that increasing the parameter γ reduces the correlation range of the strain energy function random field. This, in turn, implies shorter correlation ranges for the local stress field, for a given set of boundary conditions.

5.3. Case of a patient-specific arterial wall

In this last section, the case of an arterial wall composed by the media layer and defined by a patient-specific geometry is considered. The biological structure is subjected to an inner pressure mimicking blood pressure. Computational aspects related to the finite element implementation for such simulations can be found in [77,86]. The geometry of the inner surface was extracted from the database [87] (file ID: 0098), and volume meshing was achieved by following the methodology proposed in [88] (the Vascular Modelling Toolkit (VMTK) and GMSH meshing software [89] were notably used). The resulting mesh (see Fig. 3) is approximatively 12 mm long and consists of 297 828 cells and 432 250 nodes, leading to a total of 1 296 750 degrees of freedom. As in Section 5.2, the mean stochastic stored energy function is obtained by using the parameters fitted in Section 5.1. A cornerstone of the approach lies in the definition of the diffusion tensor $\mathbf{x} \mapsto \mathsf{H}(\mathbf{x})$, which allows sampling on the complex geometry defining the arterial wall. A methodology to achieve such a construction is introduced in the next section.

Fig. 4. Plot of the solution fields $\mathbf{x} \mapsto \Psi_1(\mathbf{x})$ (left) and $\mathbf{x} \mapsto \Psi_2(\mathbf{x})$ (right).

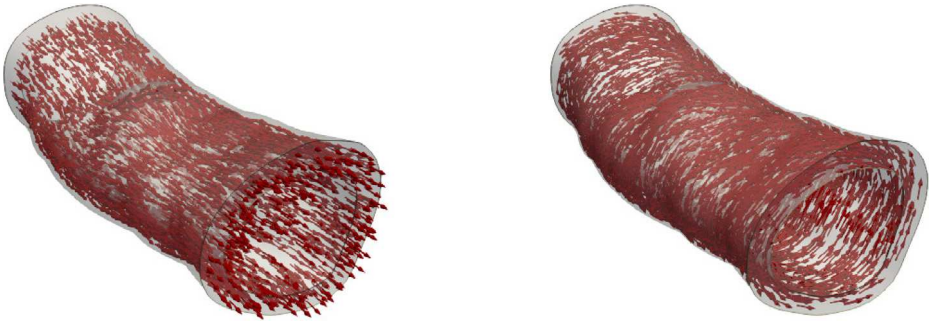

Fig. 5. Local directions $\hat{\mathbf{e}}^{(1)}(\mathbf{x})$ (left) and $\hat{\mathbf{e}}^{(2)}(\mathbf{x})$ (right) at uniformly distributed positions in the media.

5.3.1. Definition of the diffusion field on the arterial wall

For any $\mathbf{x}$ fixed in $\mathscr{B}$, the definition of a local basis $\{\hat{\mathbf{e}}^{(i)}(\mathbf{x})\}_{i=1}^3$ and preferred directions $\{\mathbf{a}^{(\ell)}(\mathbf{x})\}_{\ell=1}^2$ relevant to the arterial geometry can be performed by having recourse to the Laplace–Dirichlet Rule-Based (LDRB) algorithm proposed in [90] (and revisited, for deterministic simulations on arteries, in [91]). In this approach, two auxiliary Laplace boundary value problems are introduced in order to define local fields, denoted by $\mathbf{x} \mapsto \Psi_1(\mathbf{x})$ and $\mathbf{x} \mapsto \Psi_2(\mathbf{x})$ respectively, the gradient fields of which can be related to the aforementioned basis and directions. More precisely, the field $\mathbf{x} \mapsto \Psi_1(\mathbf{x})$ is defined as the solution of the following Laplace problem:

$$\triangle \Psi_1(\mathbf{x}) = 0 \,, \quad \forall\, \mathbf{x} \in \mathscr{B} \,, \tag{47}$$

with $\Psi_1(\mathbf{x}) = 0$ on the inlet surface and $\Psi_1(\mathbf{x}) = 1$ on the outlet surface. Similarly, Ψ_2 is assumed to satisfy

$$\triangle \Psi_2(\mathbf{x}) = 0 \,, \quad \forall\, \mathbf{x} \in \mathscr{B} \,, \tag{48}$$

and the boundary conditions write $\Psi_2(\mathbf{x}) = 0$ on the inner surface and $\Psi_2(\mathbf{x}) = 1$ on the outer surface. The plots of the solutions are shown in Fig. 4.

For $\mathbf{x}$ fixed in $\mathscr{B}$, the local basis is next defined as:

$$\hat{\mathbf{e}}^{(1)}(\mathbf{x}) := \frac{\nabla \Psi_2(\mathbf{x})}{\|\nabla \Psi_2(\mathbf{x})\|} \,, \quad \hat{\mathbf{e}}^{(2)}(\mathbf{x}) := \hat{\mathbf{e}}^{(3)}(\mathbf{x}) \times \hat{\mathbf{e}}^{(1)}(\mathbf{x}) \,, \quad \hat{\mathbf{e}}^{(3)}(\mathbf{x}) := \frac{\nabla \Psi_1(\mathbf{x})}{\|\nabla \Psi_1(\mathbf{x})\|} \,, \tag{49}$$

and the plots of the vector fields $\mathbf{x} \mapsto \hat{\mathbf{e}}^{(1)}(\mathbf{x})$ and $\mathbf{x} \mapsto \hat{\mathbf{e}}^{(2)}(\mathbf{x})$ thus defined are shown in Fig. 5. For any $\mathbf{x}$ in $\mathscr{B}$, the preferred directions (defining the local anisotropic contribution) are finally expressed as

$$\mathbf{a}^{(1)}(\mathbf{x}) = \cos(\theta)\hat{\mathbf{e}}^{(1)}(\mathbf{x}) + \sin(\theta)\hat{\mathbf{e}}^{(2)}(\mathbf{x}) \,, \quad \mathbf{a}^{(2)}(\mathbf{x}) = \cos(\theta)\hat{\mathbf{e}}^{(1)}(\mathbf{x}) - \sin(\theta)\hat{\mathbf{e}}^{(2)}(\mathbf{x}). \tag{50}$$

5.3.2. Characterization of covariance kernels on manifolds

Based on the definition of the local basis addressed in the previous section, we now investigate through numerical experiments some covariance kernels that can be generated with the SPDE approach. Without loss of generality, the

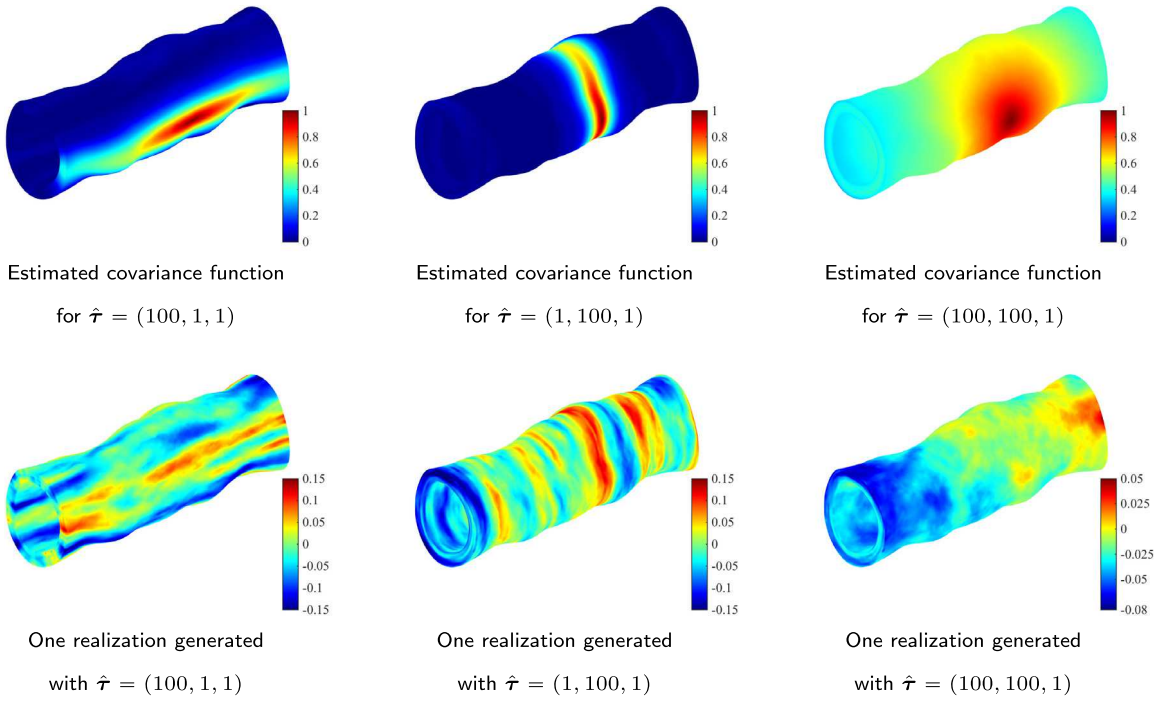

Fig. 6. Estimated covariance function and realization of the Gaussian field $\{\Xi_1(\mathbf{x}), \mathbf{x} \in \mathscr{B}\}$ ($\gamma = 3$).

stochastic properties of interest are characterized by considering the Gaussian field $\{\Xi_1(\mathbf{x}), \mathbf{x} \in \mathscr{B}\}$. The field of diffusion tensor is first defined as

$$\mathsf{H}(\mathbf{x}) := \sum_{i}^{3} \hat{\tau}_i \, \hat{\mathbf{e}}^{(i)}(\mathbf{x}) \otimes \hat{\mathbf{e}}^{(i)}(\mathbf{x}) \,, \quad \forall \mathbf{x} \in \mathscr{B} \,, \tag{51}$$

where $\hat{\tau}_1$, $\hat{\tau}_2$ and $\hat{\tau}_3$ are strictly positive parameters controlling the local anisotropy of the correlation structure. The plot of the covariance function, estimated with 4000 independent realizations of the random field (and with respect to a reference point that is arbitrarily chosen on the outer surface), and one realization of $\{\Xi_1(\mathbf{x}), \mathbf{x} \in \mathscr{B}\}$ are shown for $\gamma = 3$ and several values of $\hat{\boldsymbol{\tau}} := (\hat{\tau}_1, \hat{\tau}_2, \hat{\tau}_3)$ (see Fig. 6).

It is observed that increasing the parameter $\hat{\tau}_k$ allows for prescribing a locally anisotropic correlation structure oriented along the associated direction $\hat{\mathbf{e}}^{(k)}(\mathbf{x})$, for any k in $\{1, 2, 3\}$. In particular, selecting $\hat{\tau}_1 \gg \hat{\tau}_2$ and $\hat{\tau}_1 \gg \hat{\tau}_3$ leads to a longer correlation range along the longitudinal direction, and the associated realization thus exhibits a typical signature of this correlation pattern. Similarly, the case $\hat{\tau}_2 \gg \hat{\tau}_1$ and $\hat{\tau}_2 \gg \hat{\tau}_3$ enables one to generate a more pronounced correlation along the (local) circumferential direction. Finally, retaining $\hat{\tau}_1 = \hat{\tau}_2 \gg \hat{\tau}_3$ defines a correlation structure that is locally isotropic in the plane spanned by $(\hat{\mathbf{e}}^{(1)}(\mathbf{x}), \hat{\mathbf{e}}^{(2)}(\mathbf{x}))$. Further results involving the same directional configurations but shortest correlation ranges (obtained with a larger value of the parameter γ) are also shown in Fig. 7.

Next, the diffusion tensor field is defined as

$$\mathsf{H}(\mathbf{x}) := \kappa \, \mathsf{I} + \tau_1 \, \mathsf{M}^{(1)}(\mathbf{x}) + \tau_2 \, \mathsf{M}^{(2)}(\mathbf{x}) \,, \tag{52}$$

where $\kappa > 0$, $\tau_1 \geqslant 0$, $\tau_2 \geqslant 0$ and the structural tensors are defined with respect to the preferred orientations given by Eq. (50) (with $\theta = 46.274$ in degrees). Correlation functions and realizations of the Gaussian field are shown in Fig. 8 for $\kappa = 0.1$, $\gamma = 1$ and different values of $\boldsymbol{\tau} := (\tau_1, \tau_2)$.

As expected (following the previous numerical experiments), it is observed that selecting $\tau_i \gg \tau_j$ allows one to prescribe a signature of the anisotropy along the preferred orientation $\mathbf{a}^{(i)}(\mathbf{x})$. This feature is, in particular, relevant to situations where the random field model must account for subscale (e.g. microstructural) details. By contrast, the case

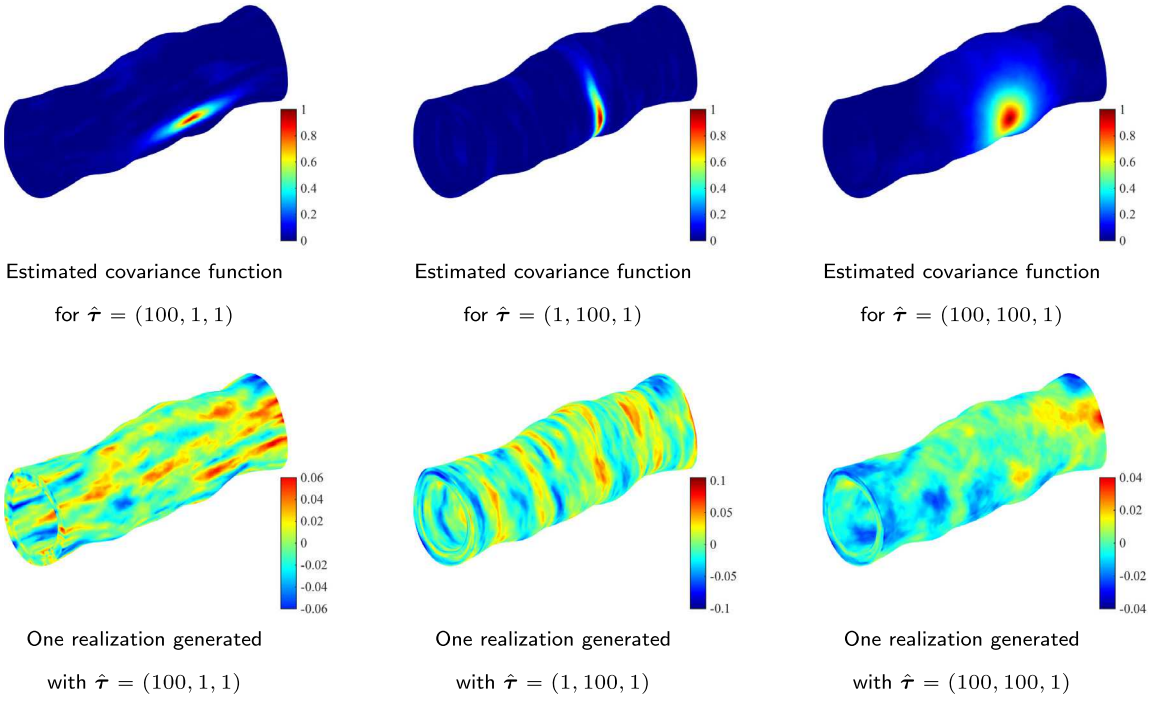

Fig. 7. Estimated covariance function and realization of the Gaussian field $\{\Xi_1(\mathbf{x}), \mathbf{x} \in \mathscr{B}\}$ ($\gamma = 10$).

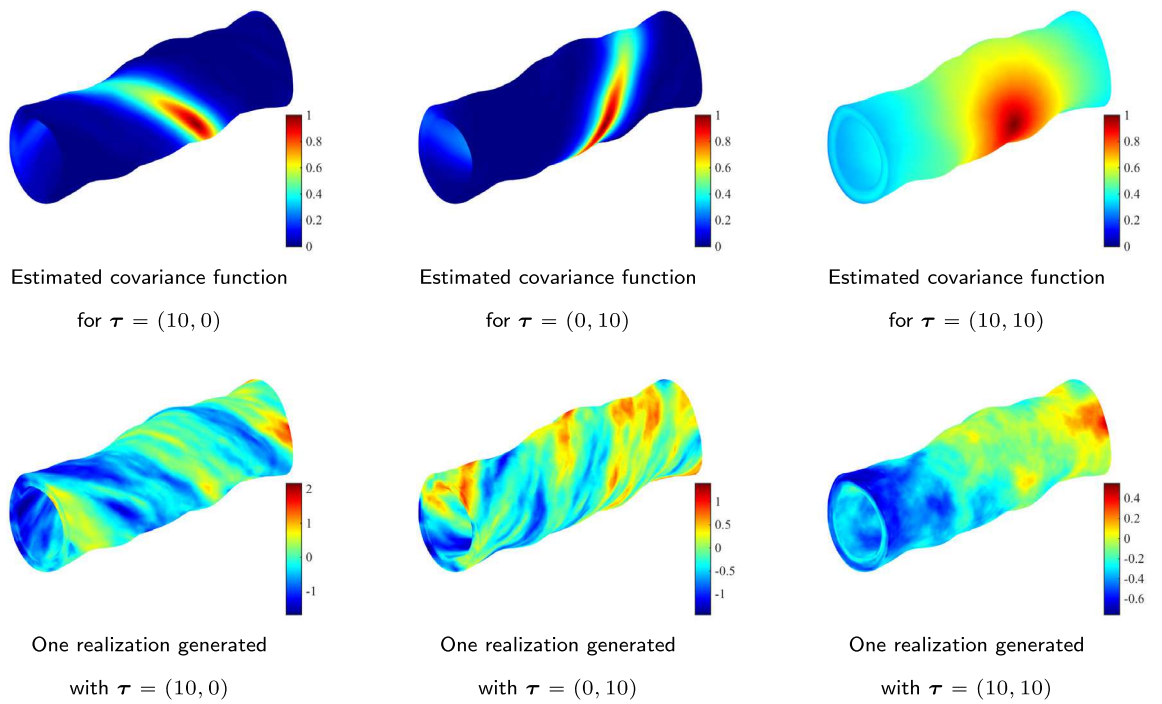

Fig. 8. Estimated covariance function and realization of the Gaussian field $\{\Xi_1(\mathbf{x}), \mathbf{x} \in \mathscr{B}\}$ ($\kappa = 0.1$, $\gamma = 1$).

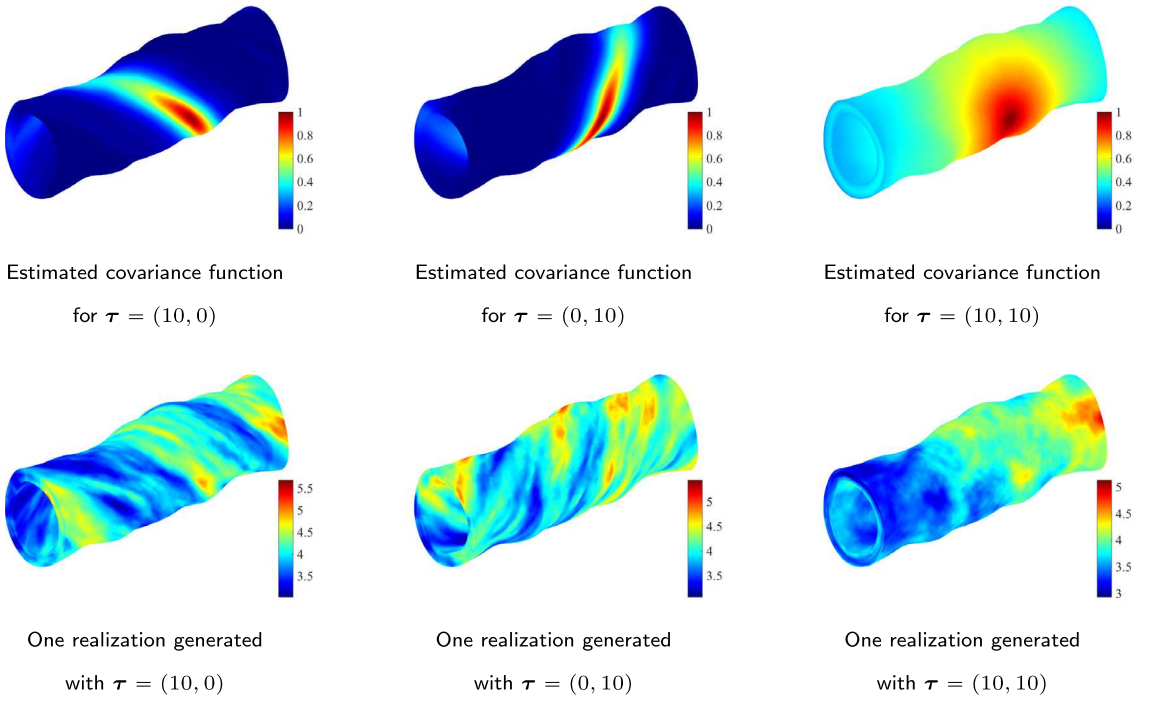

Fig. 9. Estimated covariance function and realization of the non-Gaussian field $\{G_1(\mathbf{x}), \mathbf{x} \in \mathscr{B}\}$ ($\kappa = 0.1$, $\gamma = 1$).

$\tau_1 \approx \tau_2$ leads to an isotropic correlation structure in the plane spanned by $(\mathbf{a}^{(1)}(\mathbf{x}), \mathbf{a}^{(2)}(\mathbf{x}))$. Although the conclusions presented here hold for the underlying Gaussian random field $\{\Xi_1(\mathbf{x}), \mathbf{x} \in \mathscr{B}\}$, it should be emphasized that the non-Gaussian field obtained from the point-wise transformation of this field inherits from such features, as depicted in Fig. 9 in the case of the correlation function. Finally, it should be noticed at this point that the sampling strategy can readily accommodate randomness in the geometry (see [92] for a discussion focusing on arterial walls). In this case, the diffusion field $\mathbf{x} \mapsto \mathsf{H}(\mathbf{x})$ must be constructed for each sample of domain Ω, which requires in turn the two auxiliary Laplace problems described in Section 5.3.1 to be solved.

5.3.3. *Uncertainty propagation*

In this final section, uncertainty propagation is performed by considering the random field model for anisotropic strain energy functions constructed in this work, as well as the sampling methodology presented in the previous sections. The patient-specific geometry shown in Fig. 3 is used and subjected to a 12 kPa pressure load on its inner surface. The inlet surface is totally clamped, while a sliding boundary condition is prescribed on the outlet surface (alternative boundary conditions for such applications can be found in [79]). The diffusion tensor field is defined as in Eq. (52), with $\kappa = 0.1$, $\gamma = 1$, $\tau_1 = \tau_2 = 10$ and $\theta = 46.274$ (deg). The coefficients of variation of the input random fields are all set to 0.1. Realizations of the Von Mises stress field (in terms of the Cauchy stress tensor) are shown, together with the response obtained with the nominal (mean) model, in Figs. 10 and 11.

It is seen that the fluctuations in the anisotropic strain energy functions can induce pronounced fluctuations in the Von Mises stress, especially when compared with the mean response (which is the one that is routinely considered in computational simulations for such vessels), and may thus have a strong impact on any subsequent calculation (such as the computation of a failure probability). Not surprisingly, the localization patterns in the stress distribution turn out to be rather reproducible, given the influence of the (deterministic) geometry, and reflect the signature of the underlying anisotropy (which is raised by the selected functional form). The probability density function of the maximum Von Mises stress, computed from a set of 500 independent realizations using the kernel estimation method, is finally shown in Fig. 12.

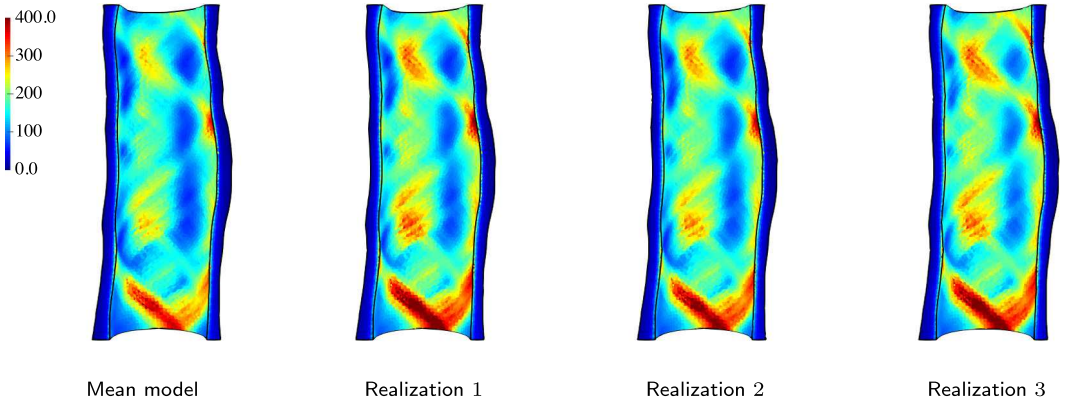

Fig. 10. Response associated with the mean model and three independent realizations of the Von Mises stress field (in kPa) on the inner surface of the arterial wall.

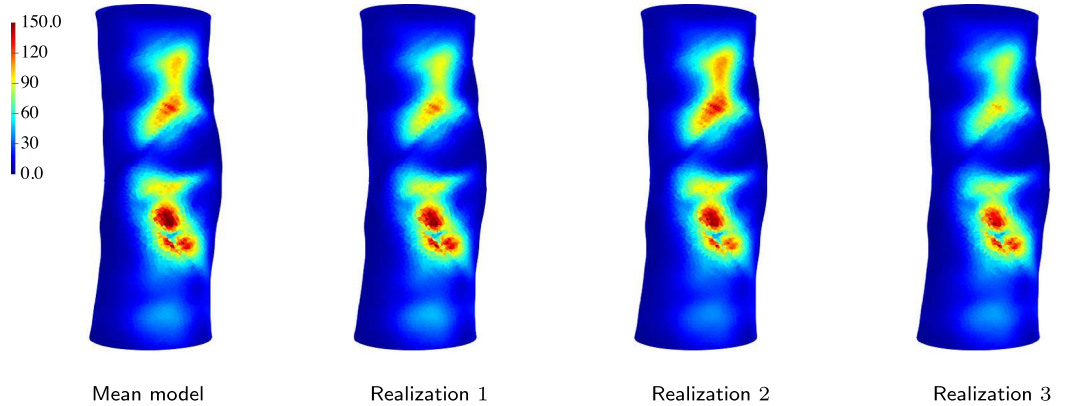

Fig. 11. Response associated with the mean model and three independent realizations of the Von Mises stress field (in kPa) on the outer surface of the arterial wall.

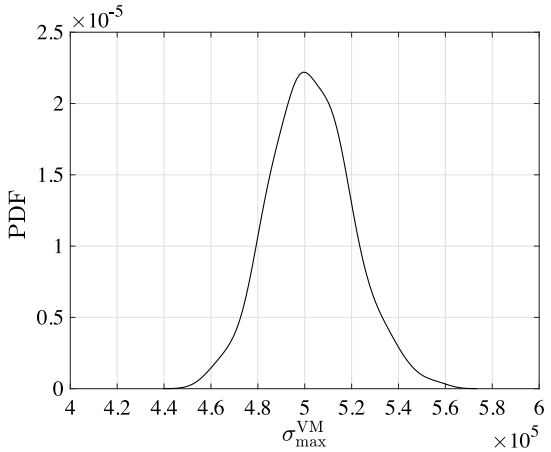

Fig. 12. Plot of the probability density function for the maximum value of the Von Mises stress (in Pa).

6. Conclusion

In this work, a random field model for a prototypical anisotropic stored energy function has been presented. The stochastic framework relies on information theory, which is invoked in order to account for the mathematical requirements raised by the functional analysis of nonlinear boundary value problems. All the samples generated through the proposed approach are hence admissible, and the probabilistic formulation introduces a limited modeling bias thanks to the entropy maximization. An efficient and robust computational methodology for sampling on complex geometries defined by smooth manifolds was additionally detailed. Various numerical applications were finally considered. In particular, the capability of the stochastic model to produce anisotropic correlation kernels and realizations with specific signatures was assessed. While technical derivations were achieved on a particular functional form, the proposed framework can readily be applied to any strain energy function of interest, as well as to other complex soft biological tissues, such as brain tissues.

Acknowledgment

This work was funded in part by the National Science Foundation under grant CMMI-1726403.

References

[1] R.G. Ghanem, D. Higdon, H. Owhadi (Eds.), Handbook of Uncertainty Quantification, Springer-Verlag, 2017.
[2] M. Ostoja-Starzewski, Microstructural Randomness and Scaling in Mechanics of Materials, CRC Press, 2007.
[3] K. Miller, K. Chinzei, Constitutive modelling of brain tissue: experiment and theory, J. Biomech. 30 (1997) 1115–1121.
[4] K. Miller, K. Chinzei, Mechanical properties of brain tissue in tension, J. Biomech. 35 (2002) 483–490.
[5] F. Velardi, F. Fraternali, M. Angelillo, Anisotropic constitutive equations and experimental tensile behavior of brain tissue, Biomech. Model. Mechanobiol. 5 (2006) 53–61.
[6] R. Roan, K. Vemaganti, The nonlinear material properties of liver tissue determined from no-slip uniaxial compression experiments, J. Biomech. Eng. 129 (2007) 450–456.
[7] M. Hrapko, J. Van Dommelen, G. Peters, J. Wismans, Characterisation of the mechanical behaviour of brain tissue in compression and shear, Biorheology 45 (2008) 663–676.
[8] R. Roan, K. Vemaganti, Strain rate-dependent viscohyperelastic constitutive modeling of bovine liver tissue, Med. Biol. Eng. Comput. 49 (2011) 497–506.
[9] C.J. Sparrey, T.M. Keaveny, Compression behavior of porcine spinal cord white matter, J. Biomech. 44 (2011) 1078–1082.
[10] B. Rashid, M. Destrade, M.D. Gilchrist, Mechanical characterization of brain tissue in compression at dynamic strain rates, J. Mech. Behav. Biomed. Mater. 10 (2012) 23–38.
[11] X. Jin, F. Zhu, H. Mao, M. Shen, K.H. Yang, A comprehensive experimental study on material properties of human brain tissue, J. Biomech. 46 (2012) 2795–2801.
[12] B. Rashid, M. Destrade, M.D. Gilchrist, Mechanical characterization of brain tissue in simple shear at dynamic strain rates, J. Mech. Behav. Biomed. Mater. 28 (2013) 71–85.
[13] S. Umale, C. Deck, N. Bourdet, P. Dhumane, L. Soler, J. Marescaux, R. Willinger, Experimental mechanical characterization of abdominal organs: liver, kidney & spleen, J. Mech. Behav. Biomed. Mater. 17 (2013) 22–33.
[14] B. Rashid, M. Destrade, M.D. Gilchrist, Mechanical characterization of brain tissue in tension at dynamic strain rates, J. Mech. Behav. Biomed. Mater. 33 (2014) 43–54.
[15] O.P. Le Maître, O.M. Knio, Spectral Methods for Uncertainty Quantification: With Applications to Computational Fluid Dynamics, Springer-Verlag, 2010.
[16] T.J. Sullivan, Introduction to Uncertainty Quantification, Springer-Verlag, 2015.
[17] R.G. Ghanem, P.D. Spanos, Stochastic Finite Elements: A Spectral Approach, revised ed., Dover Publications, 2003.
[18] N. Wiener, The homogeneous chaos, Am. J. M. 60 (1938) 897–936.
[19] R.H. Cameron, W.T. Martin, The orthogonal development of nonlinear functionals in series of fourier-hermite functionals, Ann. of Math. 48 (1947) 385–392.
[20] D. Xiu, G.E. Karniadakis, The Wiener–Askey polynomial chaos for stochastic differential equations, SIAM J. Sci. Comput. 24 (2002) 619–644.
[21] C. Soize, R.G. Ghanem, Physical systems with random uncertainties: Chaos representation with arbitrary probability measure, SIAM J. Sci. Comput. 26 (2004) 395–410.
[22] C. Soize, R.G. Ghanem, Reduced chaos decomposition with random coefficients of vector-valued random variables and random fields, Comput. Methods Appl. Mech. Engrg. 198 (2009) 1926–1934.
[23] A. Nouy, C. Soize, Random field representations for stochastic elliptic boundary value problems and statistical inverse problems, Eur. J. App. Math. 25 (2014) 339–373.
[24] M. Arnst, R.G. Ghanem, C. Soize, Identification of bayesian posteriors for coefficients of chaos expansions, J. Comput. Phys. 229 (2010) 3134–3154.
[25] C. Soize, Non-Gaussian positive-definite matrix-valued random fields for elliptic stochastic partial derivative operators, Comput. Methods Appl. Mech. Engrg. 195 (2006) 26–64.

[26] M. Grigoriu, Probabilistic models for stochastic elliptic partial differential equations, J. Comput. Phys. 229 (2010) 8406–8429.
[27] J. Guilleminot, C. Soize, On the statistical dependence for the components of random elasticity tensors exhibiting material symmetry properties, J. Elasticity 111 (2012) 109–130.
[28] J. Guilleminot, C. Soize, Stochastic model and generator for random fields with symmetry properties: Application to the mesoscopic modelling of elastic random media, SIAM J. Mult. Model. Sim. 11 (2013) 840–870.
[29] B. Staber, J. Guilleminot, Approximate solutions of Lagrange multipliers for information-theoretic random field models, SIAM/ASA J. U.Q. 3 (2015) 599–621.
[30] B. Staber, J. Guilleminot, Stochastic modeling and generation of random fields of elasticity tensors: a unified information-theoretic approach, C. R. Mécanique 345 (2017) 399–416.
[31] M.T. Nguyen, C. Desceliers, C. Soize, J.M. Allain, H. Gharbi, Multiscale identification of the random elasticity field at mesoscale of a heterogeneous microstructure using multiscale experimental observations, Int. J. Multiscale Com. 13 (2015) 281–295.
[32] T.T. Le, J. Guilleminot, C. Soize, Stochastic continuum modeling of random interphases from atomistic simulations. Application to a polymer nanocomposite, Comput. Methods Appl. Mech. Engrg. 303 (2016) 430–449.
[33] V.P. Tran, J. Guilleminot, S. Brisard, K. Sab, Stochastic modeling of mesoscopic elasticity random field, Mech. Mater. 93 (2016) 1–12.
[34] M. Malyarenko, M. Ostoja-Starzewski, A random field formulation of Hooke's law in all elasticity classes, J. Elasticity 127 (2016) 269–302.
[35] B.V. Rosić, H.G. Matthies, Stochastic galerkin method for the elastoplasticity problem with uncertain parameters, in: Recent Developments and Innovative Applications in Computational Mechanics, Springer-Verlag, 2011, pp. 303–310.
[36] M. Arnst, R.G. Ghanem, A variational-inequality approach to stochastic boundary value problems with inequality constraints and its application to contact and elastoplasticity, Internat. J. Numer. Methods Engrg. 89 (2012) 1665–1690.
[37] J. Biehler, M.W. Gee, W.A. Wall, Towards efficient uncertainty quantification in complex and large-scale biomechanical problems based on a Bayesian multi-fidelity scheme, Biomech. Model. Mechanobiol. 14 (2015) 489–513.
[38] J. Biehler, S. Kehl, M.W. Gee, F. Schmies, J. Pelisek, A. Maier, C. Reeps, H.-H. Eckstein, W.A. Wall, Probabilistic noninvasive prediction of walls properties of abdominal aortic aneurysms using Bayesian regression, Biomech. Model. Mechanobiol. 16 (2017) 45–61.
[39] B. Staber, J. Guilleminot, Stochastic modelling of a class of stored energy functions for incompressible hyperelastic materials with uncertainties, C.R. Mécanique 349 (2015) 503–514.
[40] B. Staber, J. Guilleminot, Stochastic modeling of the Ogden class of stored energy functions for hyperelastic materials: the compressible case, J. App. Math. Mech. 97 (2016) 273–295.
[41] B. Staber, J. Guilleminot, Stochastic hyperelastic constitutive laws and identification procedure for soft biological tissues with intrinsic variability, J. Mech. Behav. Biomed. Mater. 65 (2017) 743–752.
[42] R. Ghanem, D. Higdon, H. Owhadi (Eds.), Handbook of Uncertainty Quantification, Springer, Cham, 2017.
[43] P. Ciarlet, Mathematical Elasticity, vol. I: Three-Dimensional Elasticity, Elsevier Science Publishers, 1988.
[44] R.W. Ogden, Nonlinear Elastic Deformations, Dover Publications, 1997.
[45] G.A. Holzapfel, Nonlinear Solid Mechanics - A Continuum Approach for Engineering, John Wiley & Sons Ltd, 2000.
[46] G.A. Holzapfel, T.C. Gasser, R.W. Ogden, A new constitutive framework for arterial wall mechanics and a comparative study of material models, J. Elasticity 61 (2000) 1–48.
[47] T.C. Gasser, R.W. Ogden, G.A. Holzapfel, Hyperelastic modelling of arterial layers with distributed collagen fibre orientations, J. Roy. Soc. Int. 3 (2006) 15–35.
[48] G.A. Holzapfel, R.W. Ogden, Constitutive modelling of arteries, Proc. Roy. Soc. Lond. A: Math. Phys. Sc. 466 (2010) 1551–1597.
[49] G.A. Holzapfel, J.A. Niestrawska, R.W. Ogden, A.J. Reinisch, A.J. Schriefl, Modelling non-symmetric collagen fibre dispersion in arterial walls, J. Roy. Soc. Int 12 (2015) 20150188.
[50] G.A. Holzapfel, R.W. Ogden, On fiber dispersion models: Exclusion of compressed fibers and spurious model comparisons, J. Elasticity (2016) 1–20.
[51] G. Chagnon, M. Rebouah, D. Favier, Hyperelastic energy densities for soft biological tissues: a review, J. Elasticity 120 (2015) 129–160.
[52] J. Ball, Convexity conditions and existence theorems in nonlinear elasticity, Arch. Ration. Mech. Anal. 63 (1977) 337–403.
[53] B. Dacorogna, Direct Methods in the Calculus of Variations, second ed., Springer, 1989.
[54] P. Charrier, D. Dacorogna, B. Hanouzet, P. Laborde, An existence theorem for slightly compressible materials in nonlinear elasticity, SIAM J. Math. Anal. 19 (1988) 70–85.
[55] P.J. Flory, Thermodynamic relations for highly elastic materials, Trans. Faraday Soc. 57 (1961) 829–838.
[56] J. Boehler, Introduction to the invariant formulation of anisotropic constitutive equations, in: Applications of Tensor Functions in Solid Mechanics, Springer, 1987, pp. 13–30.
[57] Q.S. Zheng, Theory of representations for tensor functions –a unified invariant approach to constitutive equations, App. Mech. Rev. 47 (1994) 545–587.
[58] J. Schröder, P. Neff, Invariant formulation of hyperelastic transverse isotropy based on polyconvex free energy functions, Int. J. Solids Struct. 40 (2003) 401–445.
[59] D. Balzani, P. Neff, J. Schröder, G.A. Holzapfel, A polyconvex framework for soft biological tissues. Adjustment to experimental data, Int. J. Solids Struct. 43 (2006) 6052–6070.
[60] C. Soize, A nonparametric model of random uncertainties for reduced matrix models in structural dynamics, Prob. Eng. Mech. 15 (2000) 277–294.
[61] E. Jaynes, Information theory and statistical mechanics i., Phys. Rev. 106 (1957) 620–630.
[62] E. Jaynes, Information theory and statistical mechanics ii., Phys. Rev. 108 (1957) 171–190.
[63] C.E. Shannon, A mathematical theory of communication, Bell Syst. Tech. J. 27 (1948) 379–423/623–659.

[64] E. Chow, Y. Saad, Preconditioned Krylov subspace methods for sampling multivariate Gaussian distributions, SIAM J. Sci. Comput. 36 (2014) A588–A608.
[65] M. Shinozuka, Simulation of multivariate and multidimensional random processes, J. Acoust. Soc. of Am. 49 (1971) 357–368.
[66] F. Lindgren, H. Rue, J. Lindström, An explicit link between Gaussian fields and Gaussian Markov random fields: the stochastic partial differential equation approach, J. R. Stat. Soc. Ser. B Stat. Methodol. 74 (2011) 423–498.
[67] G.A. Fuglstad, D. Simpson, F. Lindgren, H. Rue, Exploring a new class of nonstationary spatial gaussian random fields with varying local anisotropy, Stat. Sin. 133 (2015) 25–115.
[68] G.A. Fuglstad, D. Simpson, F. Lindgren, H. Rue, Does non-stationary spatial data always require non-stationary random fields? Spat. Stat. 14 (2015) 505–531.
[69] D. Bolin, F. Lindgren, Spatial models generated by nested stochastic partial differential equations, with an application to global ozone mapping, Ann. Appl. Stat. 5 (2011) 523–550.
[70] G.A. Holzapfel, G. Sommer, P. Regitnig, Anisotropic mechanical properties of tissue components in human atherosclerotic plaques, J. Biomech. Engrg. 126 (2004) 657–665.
[71] G.A. Holzapfel, G. Sommer, T.C. Gasser, P. Regitnig, Determination of layer-specific mechanical properties of human coronary arteries with nonatherosclerotic intimal thickening and related constitutive modeling, Am. J. Phys. Heart Circ. Physiol. 289 (2005) 2048–2058.
[72] H.C. Stary, Atlas of Atherosclerosis: Progression and Regression, Parthenon Publishing Group Limited, Boca Raton, 2003.
[73] P.D. Ballyk, C. Walsh, J. Butany, M. Ojha, Compliance mismatch may promote graft-artery intimal hyperplasia by altering suture-line stresses, J. Biomech. 31 (1997) 229–237.
[74] F. Nappi, A.R. Carotenuto, A. Cutolo, P. Fouret, C. Acar, C. Chachques, M. Fraldi, Compliance mismatch and compressive wall stresses drive anomalous remodelling of pulmonary trunks reinforced with Dacron grafts, J. Mech. Behav. Biomed. Mater. 63 (2016) 287–302.
[75] G.R. Joldes, K. Miller, A. Wittek, B. Doyle, A simple effective and clinically applicable method to compute abdominal aortic aneurysm wall stress, J. Mech. Behav. Biomed. Mater. 58 (2016) 139–148.
[76] P.G. Ciarlet, The Finite Element Method for Elliptic Problems, SIAM, 2002.
[77] P. Wriggers, Nonlinear Finite Element Methods, Springer, 2008.
[78] D. Brands, A. Klawonn, O. Rheinbach, J. Schröder, Modelling and convergence in arterial wall simulations using a parallel feti solution strategy, Comput. Methods Biomech. Biomed. Engrg 11 (2008) 569–583.
[79] S. Brinkhues, A. Klawonn, O. Rheinbach, J. Schröder, Augmented Lagrange methods for quasi-incompressible materials –Applications to soft biological tissue, Int. J. Numer. Methods Biomed. Engrg. 29 (2013) 332–350.
[80] J.C. Nagtegaal, D.M. Parks, J. Rice, On numerically accurate finite element solutions in the fully plastic range, Comput. Methods App. Mech. Engrg. 4 (1974) 153–177.
[81] J.C. Simo, R.L. Taylor, K.S. Pister, Variational and projection methods for the volume constraint in finite deformation elasto-plasticity, Comput. Methods App. Mech. and Engrg. 51, 177–208.
[82] J.C. Simo, R.L. Taylor, Quasi-incompressible finite elasticity in principal stretches, continuum basis and numerical algorithms, Comput. Methods App. Mech. Engrg. 85 (1985) (1991) 273–310.
[83] M.A. Heroux, R.A. Bartlett, V.E. Howle, R.J. Hoekstra, J.J. Hu, T.G. Kolda, R.B. Lehoucq, K.R. Long, R.P. Pawlowski, E.T. Phipps, et al., An overview of the Trilinos project, ACM Trans. Math. Software 31 (2005) 397–423.
[84] M.A. Heroux, J.M. Willenbring, A new overview of the Trilinos project, Sci. Program. 20 (2012) 83–88.
[85] G.A. Holzapfel, Determination of material models for arterial walls from uniaxial extension tests and histological structure, J. Theoret. Biol. 238 (2006) 290–302.
[86] J. Bonet, R.D. Wood, Nonlinear Continuum Mechanics for Finite Element Analysis, Cambridge University Press, 1997.
[87] AneuriskWeb project website 2012, Emory University, Department of Math&CS.
[88] E. Marchandise, G. Geuzaine, J.F. Remacle, Cardiovascular and lung mesh generation based on centerlines, Int. J. Numer. Methods Biomed. Engrg. 29 (2013) 665–682.
[89] C. Geuzaine, J.F. Remacle, A 3-D finite element mesh generator with built-in pre-and post-processing facilities, Int, J. Numer. Methods Engrg. 79 (2009) 1309–1331.
[90] J.D. Bayer, R.C. Blake, G. Plank, N.A. Trayanova, A novel rule-based algorithm for assigning myocardial fiber orientation to computational heart models, Ann. Biomed. Eng. 40 (2012) 2243–2254.
[91] C. Augustin, G.A. Holzapfel, O. Steinbach, Classical and all-floating FETI methods for the simulation of arterial tissues, Int. J. Numer. Methods Engrg. 99 (2014) 290–312.
[92] L. Kelsey, C. Schultz, K. Miller, B. Doyle, The effects of geometric variation from OCT-derived 3D reconstructions on wall shear stress in a patient-specific coronary artery, in: Computational Biomechanics for Medicine: From Algorithms to Models and Applications, Cham, 2017.
[93] H. Rue, L. Held, Gaussian Markov Random Fields: Theory and Applications, CRC Press, 2005.